People's Democratic Republic of Algeria

Ministry of Higher Education and Scientific Research

University M'Hamed BOUGARA – Boumerdes

Institute of Electrical and Electronic Engineering

Department of Power and Control

Final Year Project Report Presented in Partial Fulfilment of the Requirements for the Degree of

MASTER

In **Power Engineering**

Option: **Power Engineering**

Title:

Control of Stand-Alone PV System with Global Maximum Power Point Identification

Presented by:

- **DAMOU REZKALLAH**
- **SAHEB ANIS**

Supervisor:

- **Prof. Kheldoun Aissa**

Academic Year 2024

ABSTRACT

As the world faces the depletion of fossil fuels and the adverse environmental impacts of their use, renewable energy sources have become crucial for sustainable development. Solar energy, one of the most abundant renewable resources, is harnessed using photovoltaic (PV) systems that convert sunlight into electrical energy. Despite their potential, PV systems are plagued by low efficiency and dependency on various factors such as solar irradiance, temperature, electrical load, and ambient conditions.

One of the major challenges in PV systems is partial shading, which occurs when only a portion of the PV array is obstructed from sunlight. This shading can drastically reduce the overall power output and create multiple local maximum power points (LMPs) on the power curve, complicating the optimization process.

In PV systems with partial shading, multiple LMPs and one global maximum power point (GMPP) exist. Hence, the identification of global maximum power point GMPP is needed, which is the main topic of this thesis. The project's method is applied and simulated using MATLAB and Simulink on a stand-alone photovoltaic system powered by an MPPT controller.

The suggested method (Enhanced Adaptive P&O) produced outstanding results in differentiating between uniform irradiance and partial shading occurrences under a variety of insolation levels and complex shading scenarios. A comparative study based on convergence time, and efficiency is conducted along with other well-known techniques: Particle Swarm Optimization (PSO) and Grey Wolf Optimization (GWO). The obtained results demonstrated that the EA-P&O is either excellent or competitive with respect to tracking efficiency, convergence speed and eliminate the oscillation problem.

DEDICATION

I dedicate this work to my creator Allah, my family, and my friends: my father, my mother, my sisters, and my brothers.

Especially to my father, who passed away during this Ramadan May Allah have mercy on him. He taught me everything in my life, from basic mathematics to high school mathematics, as well as daily life lessons.

He contributed to the man I am now.

He was a pillar in our family that no one can replace, and his death brings tears to my eyes and pain to my heart.

Anis SAHEB

This project is dedicated to my family, whose unwavering support and encouragement have been my constant source of strength. To my parents, for their endless sacrifices and belief in my potential, and to my friends, for their understanding and inspiration throughout this journey.

I also dedicate this work to my mentors and colleagues, whose guidance and collaboration have been invaluable.

Rezkallah DAMOU

ACKNOWLEDGMENT

All thanks to our creator Allah for His blessings and the strength He gave us to complete this project.

We would like to extend our heartfelt thanks to our supervisor, Professor Kheldoun Aissa, whose guidance and support were invaluable. He provided us with all the necessary materials, including research papers, books, and previous reports. This project would not have seen the light of the day without his presence.

We are also deeply grateful to Mr. Hamza Belmadami, who provided us with valuable resources and advice during challenging times.

Our appreciation extends to our fellow master's students who shared their experiences and offered valuable recommendations.

Lastly, we would like to acknowledge the institute IGEE, its teachers, and all employees, from those in basic functions to those in important administrative roles, for maintaining this second home for us.

Rezkallah DAMOU– Anis SAHEB

Table of contents

List of Figures

List of Tables

List of Abbreviation

PV	Photovoltaic
MPPT	Maximum Power Point Tracking
P&O	Perturb and Observe
IC	Incremental Conductance
PSCs	Partial Shading Conditions
PSO	Particle Swarm Optimization
GWO	Grey Wolf Optimizer
EA-P&O	Enhanced Adaptive Perturb and Observe
GMP	Global maximum power
DC	Direct current
AC	Alternating current
SPD	Surge Protection Devices
NiCd	Nickel Cadmium
Li-ion	Lithium-ion
DoD	Depth of discharge
SoC	State of charge
C-Rate	Charge and Discharge Rate
PWM	Pulse Width Modulation
I	Current
V	Voltage
q	The electron charge
n	Ideality factor
k	Boltzmann’s constant

T	Temperature
V_{OC}	Open circuit voltage
I_{SC}	Short circuit current
Rs	Series resistance.
Rp	Parallel resistance
KCL	Kirchoff's Current Law
KVL	Kirchoff's Voltage Law
MPP	Maximum power point
FF	Fill factor
STC	Standard test condition
AM	Air mass
η	Efficiency
Ac	Cell surface area
G	Solar irradiance
SEPIC	Single-Ended Primary-Inductor Converter
EMF	Electro-Magnetic Force
k	Duty cycle
C_o	Output Capacitor
f	Frequency
LMPP	Local Maximum Power Point
P_{best}	Personal best solution
G_{best}	Global best solution
v_i	Velocity of the ith particle
x_i	Position of the ith particle

ω	Inertia weight
C_1 & C_2	The acceleration coefficients
r_1 & r_2	Random numbers
N_P	Number of particles
X_α	The best search engine
X_β	The second best search engine
X_δ	The third best search engine
GMPP	Global Maximum Power Point
FF	Fire Fly algorithm
ACO	Ant Colony Optimization
LHS-MPP	Left-hand side of the MPP
RHS-MPP	Right-hand side of the MPP
LPP	Local Power Point
V_{LPPs}	Voltage at Local Power Points
V_{MPP}	Voltage at maximum power
D_{MPP}	Duty cycle at MPP
P	Power
L	Inductor
N	The population size

GENERAL INTRODUCTION

With the increasing global emphasis on reducing greenhouse gas emissions and advancing towards a sustainable energy future, solar energy has become an increasingly viable alternative to fossil fuels. The continuous decline in photovoltaic (PV) module prices and associated installation costs [1], have contributed to the growing adoption of solar energy systems worldwide.

Despite these advancements, the inherent variability in solar energy due to fluctuating atmospheric conditions presents significant challenges. These variations lead to substantial power losses and reduced power conversion efficiency. Consequently, effective management and optimization of PV systems are essential to maximize energy harnessing. This is where Maximum Power Point Tracking (MPPT) techniques come into play. MPPT ensures that PV systems operate at their optimal power output regardless of changing weather conditions, thereby enhancing overall efficiency without the need for additional panels or equipment.

The primary role of MPPT is to continuously adjust the operating point of the PV system to extract the maximum possible power. This optimal point is the peak of the PV panel's nonlinear current-voltage characteristic curve, influenced mainly by solar irradiance and temperature. Traditional MPPT methods, such as Perturb and Observe (P&O) and Incremental Conductance (IC), are popular due to their simplicity and ease of implementation. However, these techniques often fall short under Partial Shading Conditions (PSCs), where non-uniform solar irradiance affects different parts of the PV array, leading to multiple local minima and one maximum point in the power-voltage curve.

Addressing the limitations of classical MPPT methods under PSCs has led to the development of advanced algorithms. This project investigates the effectiveness of these techniques, focusing on Particle Swarm Optimization (PSO) and Grey Wolf Optimizer (GWO) algorithms. Additionally, the study introduces an Enhanced Adaptive P&O (EA-P&O) algorithm, specifically designed to identify the global maximum power (GMP) region under PSCs.

The main objective of this project is to explore and evaluate the performance of these advanced MPPT algorithms in accurately identifying the GMP region under various shading scenarios. This will be achieved through extensive simulation tests, assessing the tracking speed and efficiency of each algorithm.

The structure of this report is as follows:

- **Chapter 1** provides a comprehensive overview of photovoltaic systems, covering their types, key components, and the effects of solar irradiance and temperature on their performance.
- **Chapter 2** explores the basics of MPPT, reviewing classical techniques like P&O and IC, and analyzing their effectiveness through simulation studies, then an algorithm for identifying the GMPP region is proposed.
- **Chapter 3** examines advanced MPPT algorithms, including PSO, GWO, and the proposed EA-P&O, detailing their implementation and performance in achieving GMPP under partial shading scenarios.
- **General conclusion:** summarize the main points of the report and offers future work.

CHAPTER 1 : Photovoltaic systems

1.1 Introduction

Photovoltaic (PV) systems are a vital component of renewable energy, converting sunlight into electricity. This chapter provides an overview of PV systems, detailing their key components and essential functions.

Solar panels, the heart of PV systems, convert sunlight into direct current (DC) electricity. Inverters then transform this DC electricity into alternating current (AC) for use in households and the power grid. Battery storage and charge controllers are crucial for maintaining efficiency and longevity, especially in standalone systems, ensuring reliable energy supply even during non-sunny periods.

Modeling PV systems using ideal, single diode, and double diode models helps optimize design and performance, enabling a deeper understanding of PV cell characteristics. Addressing challenges like partial shading, which can significantly affect energy production, is essential. This chapter discusses solutions such as bypass diodes, which mitigate the impact of shading and preserve system efficiency.

DC-DC converters are significant in managing voltage levels and maximizing energy extraction from solar panels. The chapter covers their design and component selection, ensuring efficient and stable operation.

1.2 Types of PV systems

There exist three main types of PV systems.

1.2.1 Grid connected PV systems

They are a type of solar systems which are connected directly to the national grid, they are also called on-grid or grid tied. They are considered as the most common types of PV systems. Despite being pretty cheap compared to others type, on-grid is dependent on the national grid performance meaning that if it fails the PV system will be down as well. The components of on-grid are shown in figure 1.1 [2]

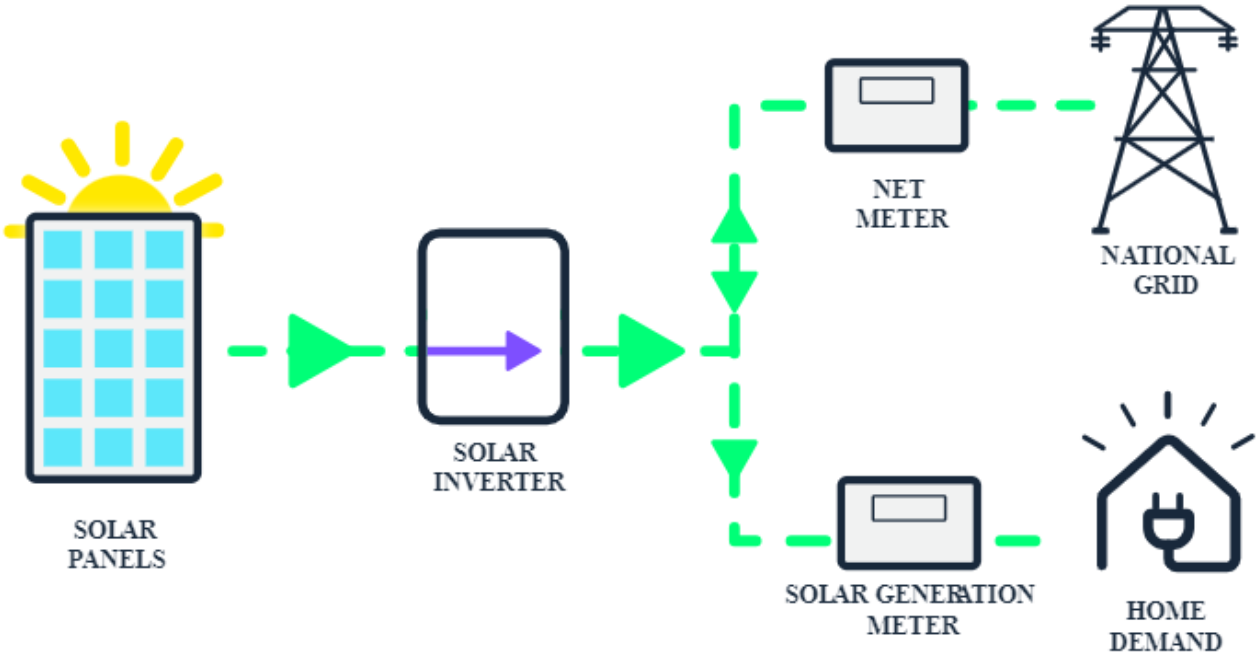

Figure 1.1: General Scheme of grid connected PV system [2].

1.2.2 Hybrid PV system

While a grid-connected PV system is dependent on the National Grid, one way to avoid this problem is by adding energy source storage (batteries) to the solar system. These batteries will act as a backup supply, storing energy and using it during grid outages (islanding mode).

Moreover, this configuration offers many advantages, such as flexibility; it draws power from the grid when the batteries are depleted and charges the batteries using cheap off-peak rates. It is a cost-effective solution because it provides an in-between option between off-grid systems and on-grid systems, meaning that it is cheaper than standalone systems but more expensive than grid-connected systems.

Despite the many benefits this configuration offers there is one main disadvantage: reduced efficiency due to the additional components involved compared to grid connected. The configuration of Hybrid PV system is shown below (figure 1.2) [2].

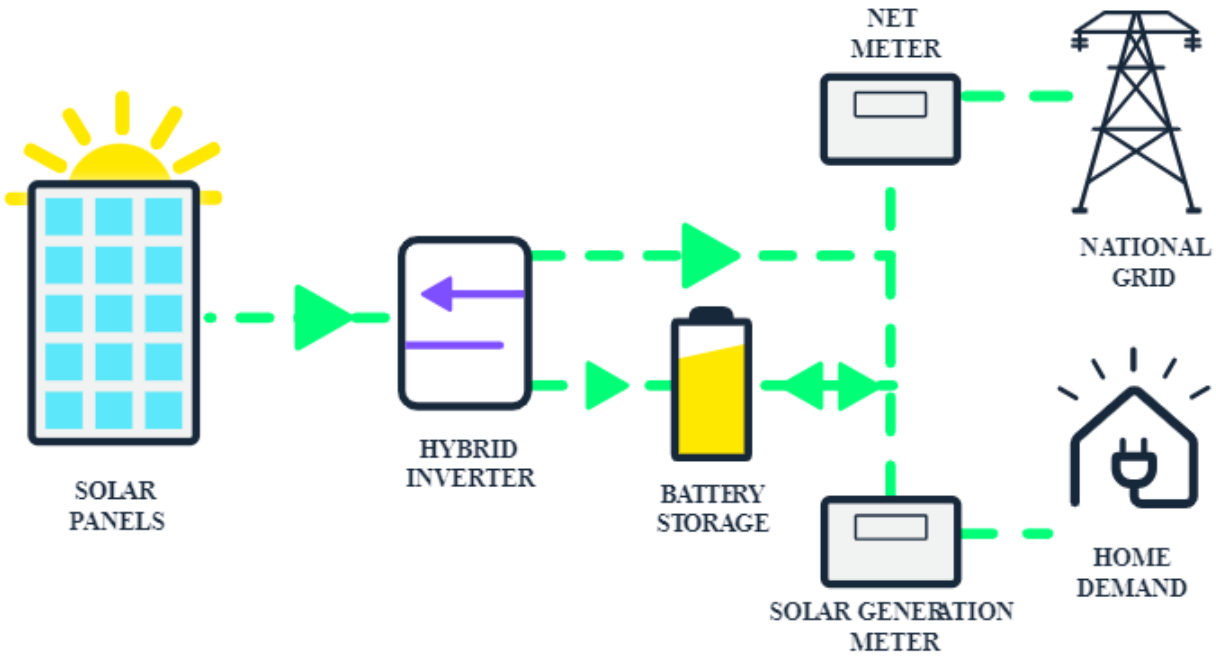

Figure 1.2: General Scheme of Hybrid PV system [2].

1.2.3 Stand-alone PV system

A stand-alone system, as its name suggest, is completely independent of the National Grid, making it ideal for areas that cannot connect to the Grid or that are difficult to connect, or for peoples who are willing to be energy independent and produce their own electricity. The benefits of such a system are numerous, including no more energy bills to pay, which were rising in the recent years, self-sufficiency meaning one can produce their own electricity even in remote location like the south of Algeria (Sahara). However, the additional components needed in this system (more batteries and backup generators) increase the overall cost of an off-grid system, making it more expensive that grid-tied and hybrid systems. Figure 1.3 shows the general scheme of stand-alone systems [2].

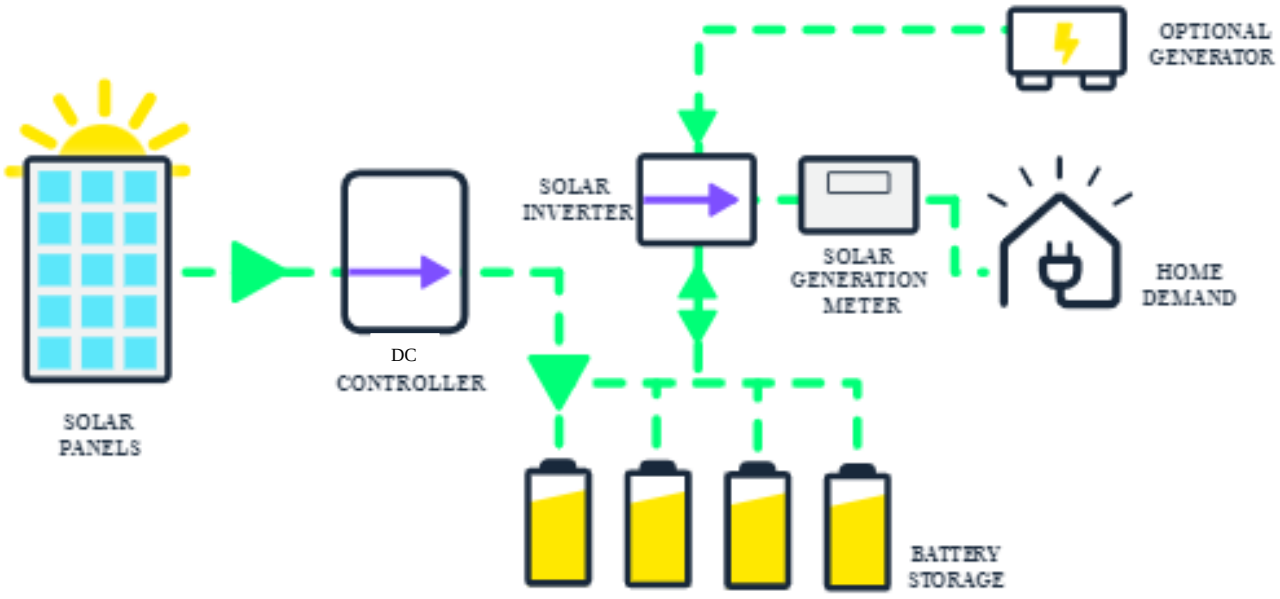

Figure 1.3: General Scheme of Stand-alone PV systems [2]

1.3Advantages and Disadvantages of PV systems

1.3.1 Advantages

- Solar energy is nearly universally available wherever sunlight is present.
- Produces energy that is both clean and silent, eliminating noise pollution.
- Addresses energy demand effectively during peak times.
- Eco-friendly, helping to preserve the environment.
- PV panels generate electricity directly via the photoelectric phenomenon.
- Systems can be customized to any size based on consumer power needs.
- Requires minimal maintenance due to the absence of moving mechanical parts.
- Economically attractive, with the cost of solar panels rapidly declining and expected to continue this trend.
- Has low operating and maintenance expenses compared to other energy systems.

1.3.2 Disadvantages

- Relies on solar availability, with no power output at night and reduced output during cloudy or rainy weather.
- Less dependable due to the variability and unpredictability of solar energy.
- Manufacturing PV panels involves toxic chemicals.
- PV systems are delicate and can be easily damaged.
- Efficiency levels of solar panels are relatively low (between 14%-25%) compared to other energy systems.
- Requires extra equipment like inverters to convert DC to AC and batteries for storage, which increases the overall investment cost significantly.
- Demands a considerable amount of space for installation.

1.4 PV system components

A PV system is constituted by many component, the most basic ones are Solar panels, Inverter, Batteries storage, and charge controllers. In this section we are going to view each component briefly.

1.3.1 Solar Panels

The heart of a solar electric system is the solar panel itself. It contains three main building blocks namely: solar cells, modules, and arrays.

A Solar cell is a semiconductor device that directly converts sunlight into electricity. It converts sunlight into electricity through photovoltaic effect; hence, it is also called photovoltaic cell. [3]

Once sunlight strikes the PV cell, some photons are absorbed by the semiconductor materials, releasing electrons from the negative layer, as depicted in Figure 1.4. These freed electrons then travel through an external circuit to the positive layer, generating an electric current, as illustrated in Figure 1.4 [4].

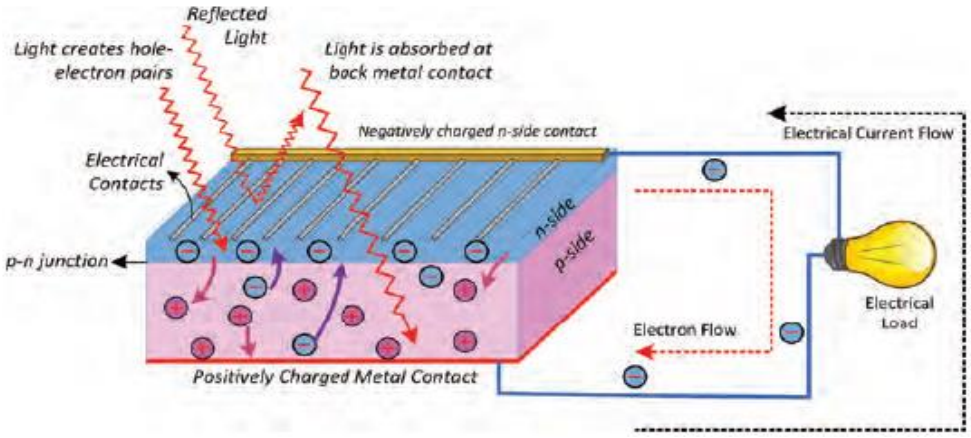

Figure 1.4: Creation of hole-electron pairs and electrical current flow through an external circuit [4].

A single solar cell is not enough to produce power that can operates a load; therefore, multiple solar cells are connected together to make a PV module. The modules are then assembled in series to create PV strings. The PV strings are wired in parallel to create photovoltaic arrays. Multiple PV arrays are brought together to form a utility PV farm. Figure 1.5 showcases this configuration.

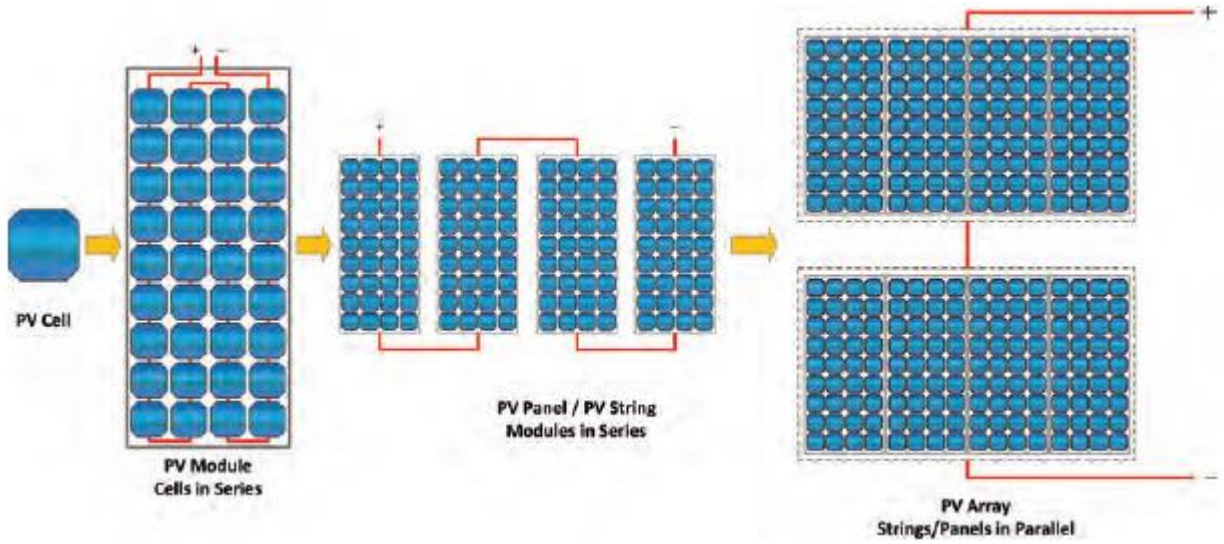

Figure 1.5: The PV cell, module, panel, and array for field applications [4].

Solar panels can be connected either in series or parallel, when connected in series Array runs at higher voltage. On the other hand, when connected in parallel, the arrays produce more power while maintaining the same voltage as the individual panels.

Solar PV technology can be divided into three main types based on the materials used to manufacture the panels: wafer-based crystalline silicon, thin-film and multi-junction concentrating PV cells, in addition to new emerging PV technologies as shown in Figure 1.6.

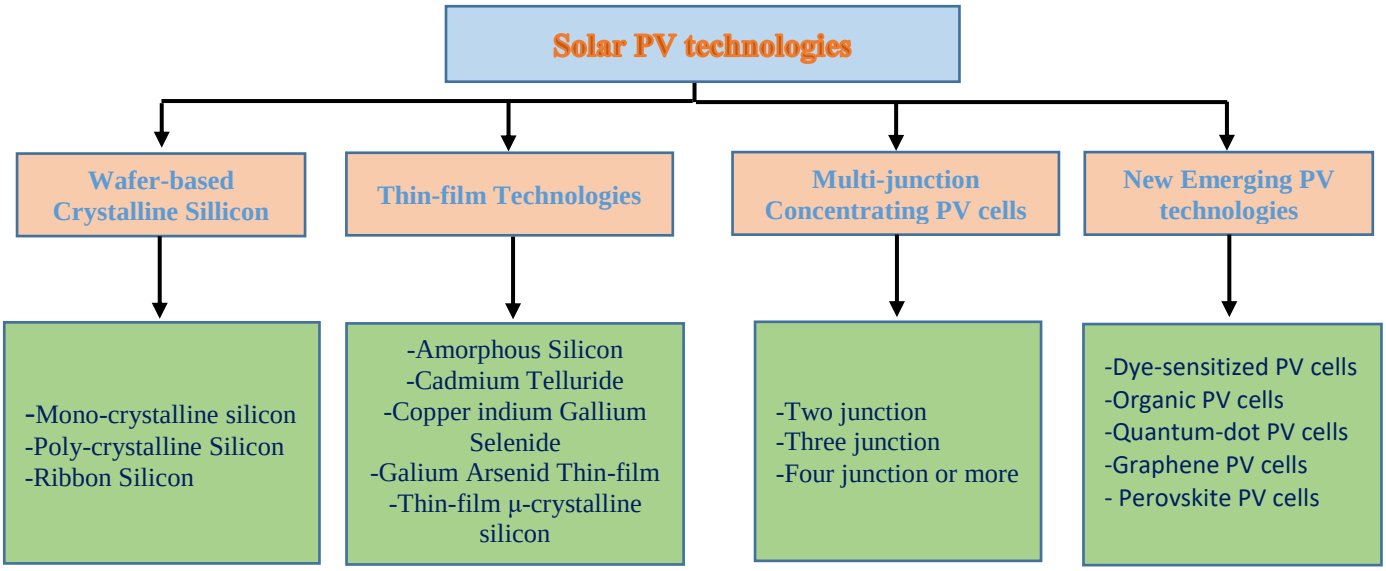

Figure 1.6: Classification of solar PV technologies [4].

1.3.2 Inverter

Most appliances around us operate on AC power, while PV modules generate DC power. Therefore, it is essential to convert DC power to AC power before using it to run these appliances. In standalone solar PV systems, energy is stored in batteries as DC power. To use the stored energy from the batteries, we must convert the DC power to AC power for the appliances. This conversion from DC to AC power is accomplished using devices known as inverters. These devices are important interface between PV panels and the loads and depending on whether or not a battery is used inverters can be categorized into three main types: grid-tied inverters, stand-alone inverters, and bimodal (battery-based interactive) inverters [3].

1.3.2.1 Grid-tied inverters

These inverters are connected to the grid and do not include battery backup. They feature specialized circuitry to synchronize the inverter's output voltage and frequency with the grid. The grid serves as a backup when the power generated by the PV array is insufficient. Additionally, these inverters have built-in MPPT to optimize power extraction from the PV array. When the sun is shining and the PV array generates more power than needed, the excess power is supplied to the grid. If the PV array produces less

power than required, the deficit is supplemented by drawing power from the grid [3]. Figure 1.7 shows the block diagram of a PV central inverter connected to the grid.

1.3.2.2 Stand-alone inverters

The basic structure of a stand-alone inverter (off-grid inverter) for PV system applications is illustrated in Figure 1.8. The key components of a stand-alone PV system include the photovoltaic array, power conditioning units (such as control equipment, charger, and MPPT), DC disconnect, AC disconnect, energy storage, and the loads. The operation of stand-alone inverters can be summarized as follows: During the day, the system converts energy from both the battery and PV array to satisfy load demands while simultaneously charging the battery. At night, the system converts stored battery energy to power the loads through the inverter [4].

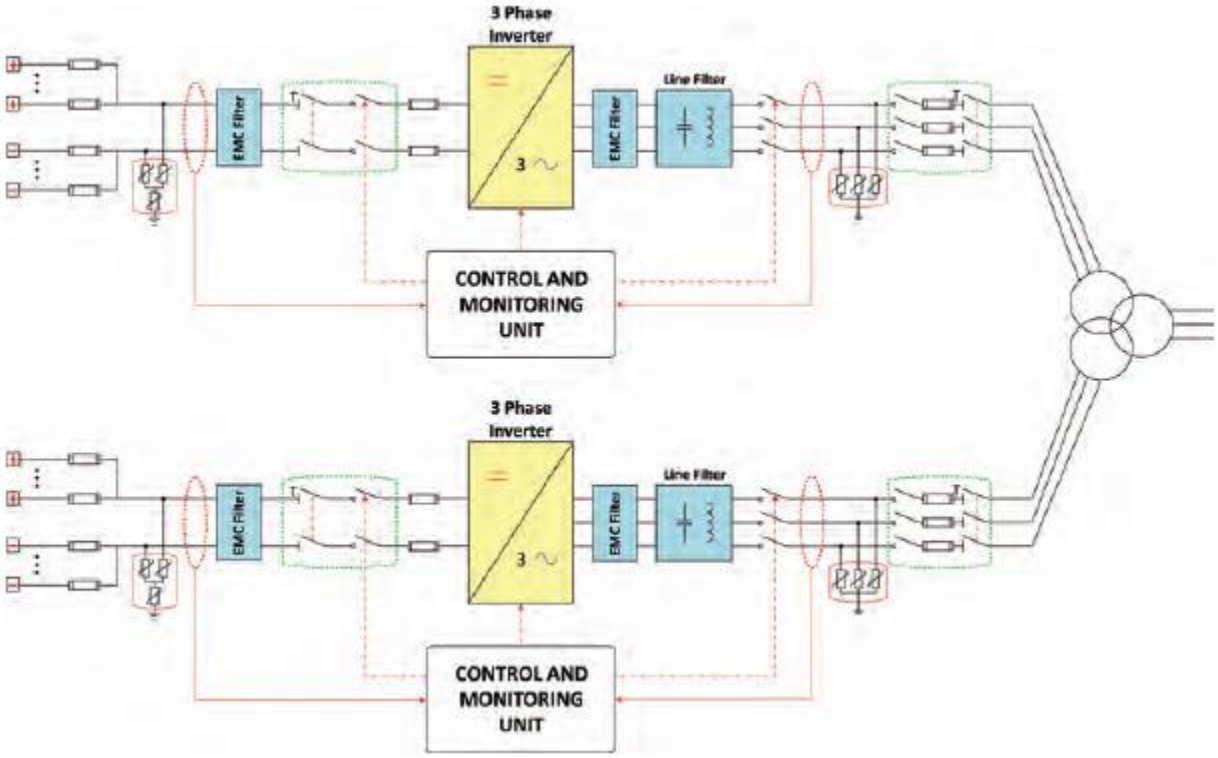

Figure 1.7 Block diagram of PV central inverter and its grid connection via a three-winding transformer [4].

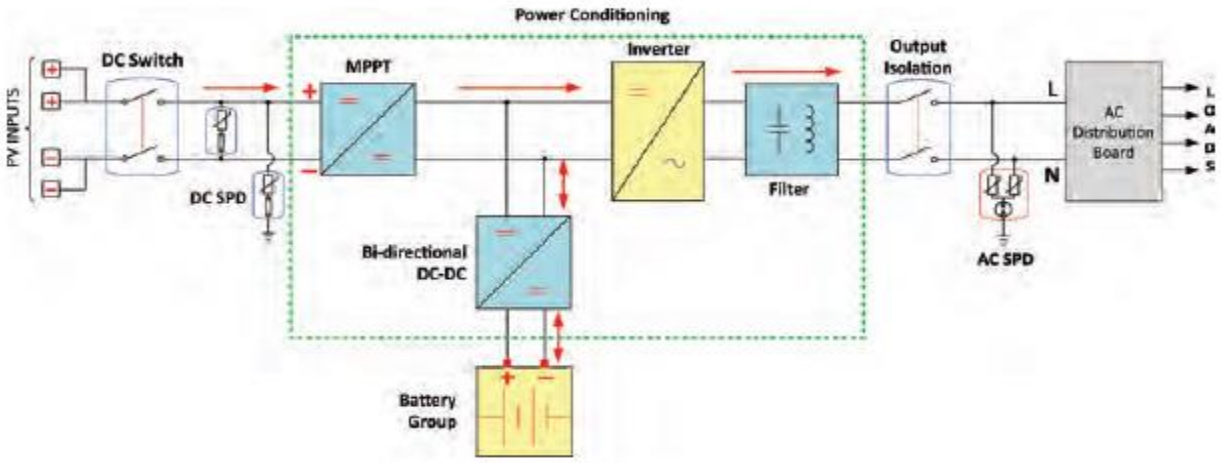

Figure 1.8 Block diagram of a stand-alone inverter with auxiliary components [4].

1.3.2.3 Bimodal inverters

Hybrid (bi-directional) solar inverters are designed to function both in stand-alone mode and when connected to the grid. The typical structure of a bimodal inverter for PV system applications is shown in Figure 1.9. During the day, any excess energy is transferred to the grid once the batteries are fully charged and the load demand is met. After sunset, the batteries continue to provide power to the AC load. If the battery cannot meet the load demand, power will be drawn from the grid. In the event of a grid failure, the system automatically switches to islanding mode, using stored battery energy and PV energy as long as they are available [4].

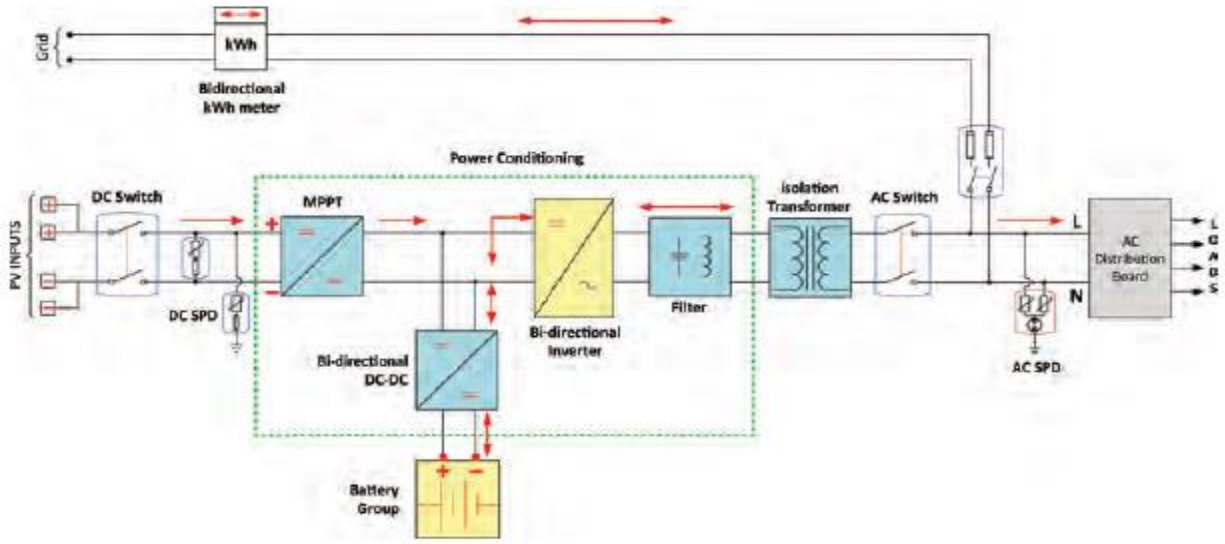

Figure 1.9 Block diagram of a bi-directional (hybrid or bimodal) inverter with auxiliary components [4].

1.4.3 Batteries storage

Batteries play a crucial and sensitive role as the energy storage medium in standalone solar PV systems. They are essential because, without energy storage, a solar PV system cannot supply power to the load during periods without sunlight. In standalone systems, electrical energy is needed to power appliances during non-sunlight hours. However, in grid-connected PV systems, energy storage isn't necessary since the grid can provide power whenever needed. In standalone PV systems, batteries are sensitive because improper or suboptimal use can significantly shorten their lifespan. Nowadays, as the cost of solar PV modules continues to decrease, the cost of batteries is becoming a more substantial portion of the overall solar PV system cost. Therefore, from a cost perspective, batteries are increasingly important in solar PV systems [3].

There are different types of batteries namely:

- Lead-Acid battery.
- Nickel Cadmium (NiCd) battery.
- Lithium-ion (Li-ion) battery.
- Other types like of fuel cell and hydrogen.

In order to select the suitable battery type, some crucial parameters must be taken into consideration:

- Battery life cycle.
- Battery cost.
- Battery efficiency.
- Battery performance under operating conditions.
- Battery capacity.
- Battery voltage.
- Depth of discharge (DoD) and State of charge (SoC).
- Charge and Discharge Rate (C-Rate).
- Battery temperature coefficient.

1.4.4 Charge Controller

Charge controllers manage the flow of charge to and from the battery, ensuring its protection by preventing overcharging and deep discharging. To preserve battery life and performance, charge controllers disconnect the battery from the circuit when it is fully charged, stopping further charging. Similarly, when a battery is excessively used and risks deep discharge, the charge controller disconnects it from the circuit to prevent further current draw. By doing so, charge controllers protect the battery from conditions that could damage it and reduce its lifespan [3].

There exist two main types of charge controllers used today:

- Pulse Width Modulation (PWM) charge controller.
- Maximum Power Point Tracking (MPPT) charge controller.

Table 1.1 Comparison of PWM Chargers and MPPT Chargers (PWM versus MPPT) [4].

PWM-Based Charge Controller	MPPT-Based Charge Controller
PV array and battery voltages must comply with each other.	Array voltage must be higher than the battery voltage. PV array voltage can be even much higher than the battery voltage.
They are generally rated for 12, 24, and 48 volts.	They have a wider input voltage range: 48–600 VDC
They have a lower ampere capacity (up to 60 A).	They have a higher ampere capacity (up to 100 A).
They are inexpensive and compact.	They are more expensive and physically larger.
They are typically recommended for use in a smaller system where boost benefits are minimal.	They can be recommended for 200 W or higher powers to take the advantage of boost benefits more.
They have relatively lower efficiency.	They are more efficient up to 30%.

1.4.5 Other components

Aside from the main components mentioned in the above subsection, there exists other components which are important as well:

- Protection devices: they ensure safety of the PV system and protect it from electrical faults as fuses, circuit breakers and surge protection.
- Monitoring systems: they track the performance and efficiency of the PV system and provide real-time data on system status, energy production and alerts for maintenance needs.
- Combiner box: combine the output of multiple strings of solar panels into single output.
- Mounting systems: there are 3 types: roof-mounted, ground- mounted and pole-mounted systems which purpose is to attach securely solar panels.

1.5 PV modeling

Various electrical and environmental factors influence the performance of a photovoltaic system. Accounting for all PV system parameters in a single model adds to the complexity and makes finding a solution more difficult. In this section we are going to move from an ideal model to single diode model and double diode model [4].

1.5.1 Ideal model

It is the simplest model, it consists of a current source in parallel with a real diode as shown in Figure 1.10.

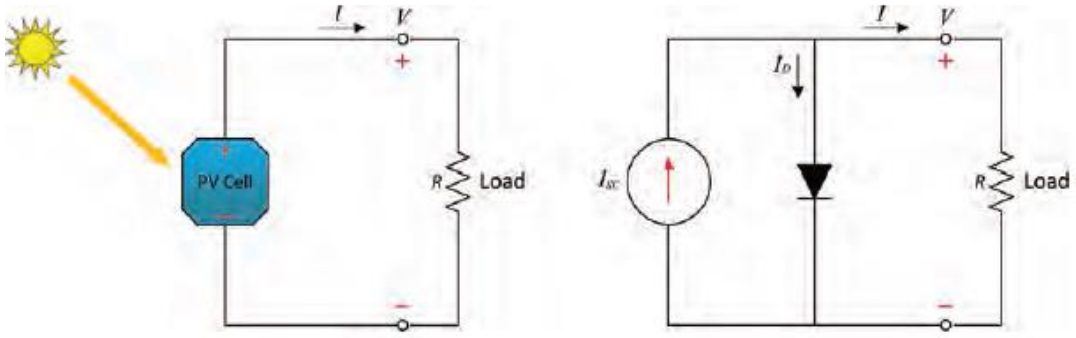

Figure 1.10: Ideal circuit model for a PV cell [4].

Using Kirchhoff's law (KCL and KVL) we can find the following equations:

$$I = I_{SC} - I_D \quad (1.1)$$

Such that:

I: the current flowing through the load (A)

I_{SC}: the short circuit current produced by the PV panel (A)

I_D: the diode current (A)

Replacing the diode current equation into 1.1 we get the following:

$$I = I_{SC} - I_0 \left(e^{\frac{q V_D}{nkTc}} - 1 \right) \quad (1.2)$$

Where:

I_0: The reverse saturation current (A).

q: The electron charge (1.602×10^{-19} C).

V_D: The voltage across the diode terminals (V).

n: Ideality factor generally between 1 and 2 ($2 \geq n \geq 1$).

k: Boltzmann's constant (1.381×10^{-23} J/K).

T_C: Junction Temperature (K).

From equation 1.2, one can extract the two main characteristics of PV system (open circuit voltage V_{OC} and short circuit current I_{SC}).

- When $V=V_D=0$, the output current I equals the short circuit current I_{SC}.
- The open-circuit voltage V_{OC} can be solved when I = 0 (equation 1.3).

$$V_{OC} = \frac{nkT_C}{q} \times \ln\left({}^{I_{SC}}/_{I_0} + 1 \right) \quad (1.3)$$

1.5.2 Single diode model

A more commonly used model is the single diode model which is more accurate than the previous model because it takes into consideration the physical phenomena affecting the PV cells like the contact and semiconductor resistances represented by Rs as well as the parallel leakage resistance represented by Rp.

Such that:

- Rs: The series resistance.
- Rp: The parallel resistance.

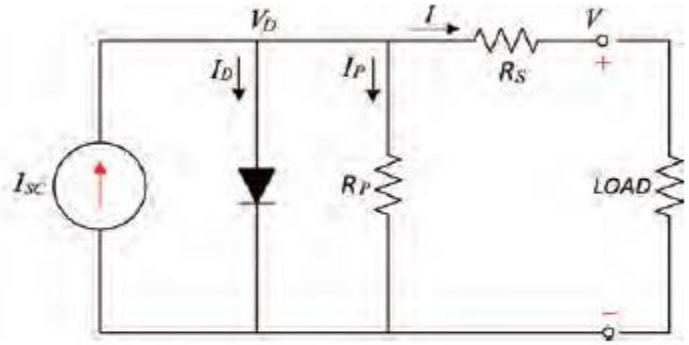

Figure 1.11 single diode model for a PV cell [4].

Using KCL and KVL, the single diode model equation can be derived (equation 1.4):

$$I = I_{SC} - I_0 \left(e^{q\left(\frac{V+IRs}{nkTc}\right)} - 1\right) - \frac{V + IRs}{Rp} \tag{1.4}$$

1.5.3 Two diode model

A more accurate model than the previous one is the double diode model (or two diode model) because it takes more into consideration the effect of recombination, however it is much more complicated than the single diode model due to the fact the solution is harder to find and takes more time. A representation of the model can be seen in figure 1.12 and its equation is demonstrated in equation 1.5.

$$I = I_{SC} - I_{01} \left(e^{q\left(\frac{V+IRs}{n1kTc}\right)} - 1\right) - I_{02} \left(e^{q\left(\frac{V+IRs}{n2kTc}\right)} - 1\right) - \frac{V + IRs}{Rp} \tag{1.5}$$

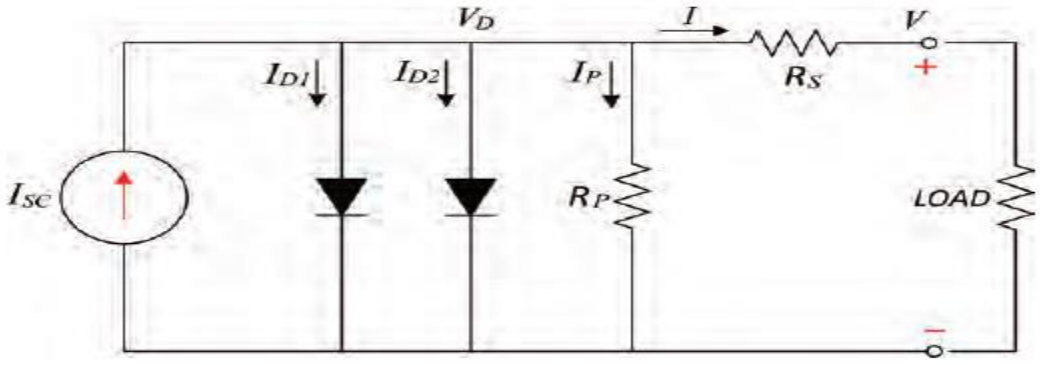

Figure 1.12: Two-diode circuit model for a PV cell [4].

1.6 PV cell characteristics

PV cells have 3 main points that characterize them: short circuit current I_{SC}, open circuit voltage V_{OC}, and maximum power point MPP. These points can be clearly seen from figure 1.13 where the P-V and I-V curve are plotted, and they are generally given in the datasheet provided by the manufacturer alongside other parameters like fill factor (FF), and efficiency of cell under standard test condition (STC). STC means that the PV cells are tested under solar radiation of 1000 W/m^2 for solar spectrum at an air mass ratio of 1.5 (1.5 AM) and temperature of 25°C.

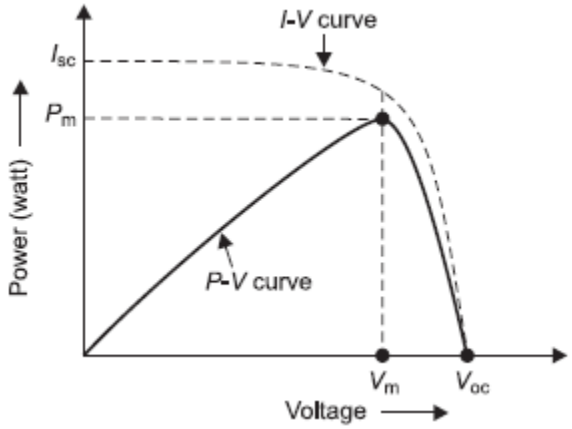

Figure 1.13 P-V and I-V curves of PV module [3].

- Short circuit current I_{SC}: The maximum current provided by the PV array when the output connectors are shorted together.
- Open circuit voltage V_{OC}: This is the maximum voltage that the array provides when the terminals are not connected to any load. It can be computed using equation 1.3.
- Maximum power point MPP: is the maximum power that a solar PV module can produce under STC.
- Fill Factor FF: The fill factor is the relationship between the maximum power that the array can actually provide under normal operating conditions and the product of the open-circuit voltage multiplied by the short-circuit current, This fill factor value gives an idea of the quality of the array and the closer the fill factor is to 1 (unity), the more power the array can provide. Typical values are between 0.7 and 0.8.

$$FF = \frac{P_{max}}{V_{OC}\, I_{SC}} \tag{1.6}$$

- Power conversion efficiency (η): the efficiency of a photovoltaic array is the ratio between the maximum electrical power that the array can produce compared to the amount of solar irradiance hitting the array.

$$\eta = \frac{P_{max}}{V_{OC}\, I_{SC}} = \frac{V_{OC}\, I_{SC}\, FF}{A_C\, G} \tag{1.7}$$

Such that, Ac: cell surface area and G: is the incoming solar radiation.

1.7 Partial Shading

Partial shading occurs when only a portion of a PV module or array is obstructed from sunlight by objects such as trees, buildings, or clouds. This uneven exposure can significantly impact the system's performance.

When a PV module is partially shaded, the output power decreases because shaded cells produce less current. This leads to a phenomenon called the "hot spot effect," where shaded cells overheat, potentially causing damage [5]. Additionally, partial shading alters the I-V characteristics of the PV array, creating multiple peaks in the power curve, complicating the power optimization process (figure 1.14).

To mitigate the effects of partial shading, bypass diodes are integrated into PV modules. These diodes allow current to flow around the shaded cells, preventing them from overheating and maintaining a higher power output. Typically, bypass diodes are placed across small groups of cells within a module, ensuring that even if some cells are shaded, the rest can continue to operate efficiently.

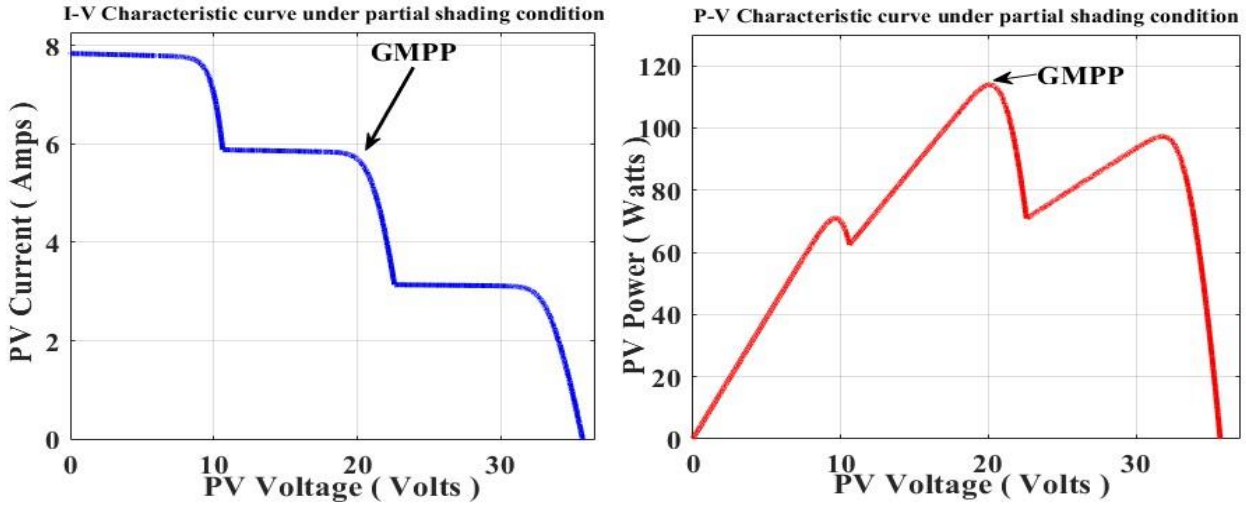

Figure 1.14: P-V and I-V curves under partial shading condition.

1.8 DC-DC converters

1.8.1 Introduction

In various industrial applications, there is often a need to transform a fixed-voltage DC source into a variable-voltage DC source. A DC-DC converter, which performs this conversion, is simply to as choppers or simply DC converter. This type of converter can be likened to a DC equivalent of an AC transformer with a continuously adjustable turns ratio. Similar to a transformer [6], a DC converter can be utilized to either step down or step up a DC voltage source.

DC-DC converters are crucial in PV systems, where they serve multiple roles, including acting as charge controllers, maximum power point trackers, and interfacing the PV source with various types of loads. Additionally, these converters are employed for noise isolation, power bus regulation, and current boosting in DC circuits.

DC-DC converters operate in two distinct modes: continuous mode and discontinuous mode. In continuous mode, the ON and OFF stages are managed so that the current in the inductor never drops to zero. Conversely, in discontinuous mode, the current in the inductor does reach zero at some point during the operation.

There exist three main configuration for DC-DC converters:

- Buck Converter (Step-Down Converter): Reduces the input voltage to a lower output voltage.
- Boost Converter (Step-Up Converter): Increases the input voltage to a higher output voltage.
- Buck-Boost Converter: Can either increase or decrease the input voltage.

Besides the three main configuration, there are three others configuration worth mentioning:

- Cuk Converter: Provides an output voltage that is either higher or lower than the input voltage, with the added benefit of a non-inverting output.
- SEPIC (Single-Ended Primary-Inductor Converter): Similar to the Cuk converter, provides an output voltage that can be higher or lower than the input voltage with non-inverting output.
- Flyback Converter: Provides isolation between input and output and can either step-up or step-down the voltage.

1.8.2 Step-up converter

Since boost converter is more used in PV systems to increase the voltage to match the load or grid requirement. This section will focus on the topology of step-up converter (figure 1.15), its working principle and its basic equation.

The fundamental operation of a step-up converter can be explained as follows:

When the switch is activated (mode 1), the boost converter circuit simplifies to the one shown in Figure 1.15.b. The current I_L flows from the source to the inductor, where energy is accumulated and stored.

When the switch is deactivated, the circuit changes to the configuration shown in Figure 1.15.b (mode 2). Due to the inductor's opposition to sudden changes in current, its EMF is reversed, adding its voltage to the input voltage. The stored energy in the inductor begins to decrease, and the current flows through the inductor, the diode, and the load, thereby charging the capacitor.

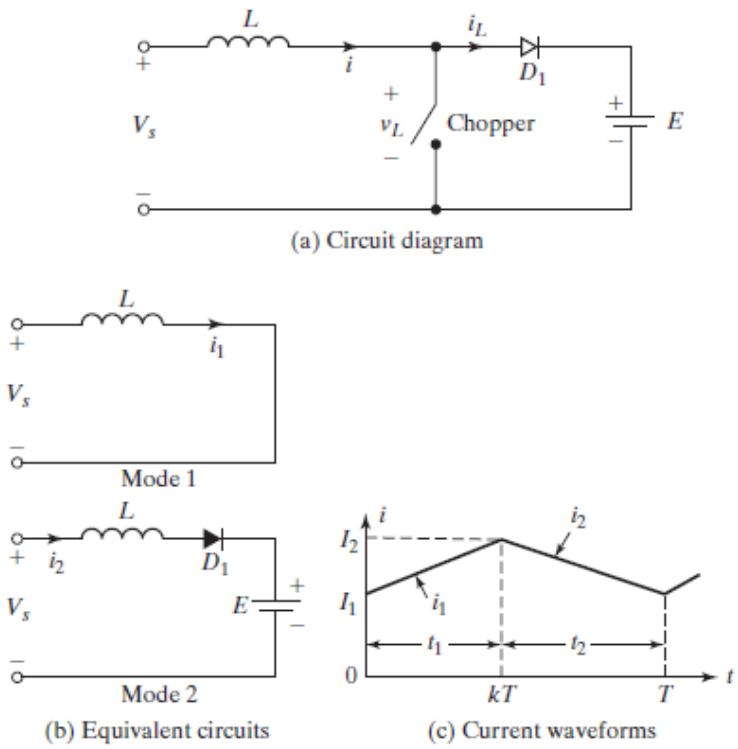

Figure 1.15: The Boost Converter: (a) Circuit diagram; (b) Equivalent circuit for the switch closed (mode 1) and open (mode 2); (c) current waveform [6].

When the switch is closed figure 1.15.b (mode 1), the voltage across the inductor is:

$$V_L = L\frac{di}{dt} \tag{1.8}$$

From t=0 to t=kT or just $t=t_1$ (mode 1):

$$V_L = L\frac{\Delta I}{t_1} \tag{1.9}$$

Such that,

$$\Delta I \ = \ I_2 - \ I_1 \tag{1.10}$$

ΔI is the peak-to-peak ripple current.

From equation.9, we can easily deduce the peak-to-peak ripple current in the inductor as

$$\Delta I = \frac{V_S}{L}t_1 \tag{1.11}$$

The average output voltage is:

$$v_0 = \ V_S + L\frac{\Delta I}{t_2} = V_S\left(1 + \frac{t_1}{t_2}\right) = \ V_S\left(\frac{1}{1-k}\right) \tag{1.12}$$

Such that k is the duty cycle of the converter bounded by zero and one $k \in [0,1]$ as shown in figure 1.16.

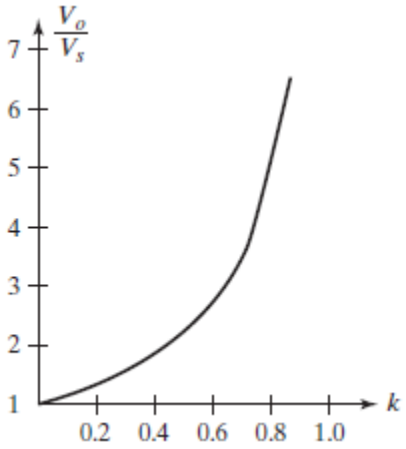

Figure 1.16: The Boost Converter output voltage [6].

One important remark that can be deduced from the above figure 1.16 is that the output voltage would be very sensible for values of k approaching one. Hence the value of the duty cycle must be maintained below its limit to avoid high conduction and switching losses that results in decrease of the overall efficiency.

1.8.3 Induction selection

Assuming no power loss in this converter meaning that the average power absorbed equal the average power supplied.

$$P_S = P_O \Rightarrow V_S I_L = \frac{V_O^2}{R} = \frac{V_S^2}{(1-k)^2 R} \tag{1.13}$$

Thus the average inductor current is:

$$I_L = \frac{V_s}{(1-k)^2 R} \tag{1.14}$$

To ensure the continuous current mode of the chopper, the inductor current must be kept positive (continuous) during its period T. In order to achieve that, the following constraint must be satisfied:

$$I_{min} = I_L - \frac{\Delta i_L}{2} > 0 \quad \Rightarrow \quad \frac{V_s}{(1-k)^2 R} - \frac{V_s kT}{2L} > 0 \tag{1.15}$$

Therefore the minimum inductance that satisfies the above constraint is:

$$L = \frac{k(1-k)^2}{2f} \tag{1.16}$$

1.8.4 Selection of the output capacitor

The selection of C_o primarily hinges on the peak-to-peak output ripple voltage, which occurs because the capacitance has a finite value in real-world applications. During the On state, the current flowing through the capacitor can be represented as:

$$I_c = C_o \frac{\Delta V_o}{T_{on}} \tag{1.17}$$

Which implies

$$C_o = \frac{k I_o}{\Delta V_o} \tag{1.18}$$

Thus, the ideal output capacitance can be determined using:

$$C_o \geq \frac{k}{R(\Delta V_o / V_o) f} \tag{1.19}$$

Such that, f is the switching frequency.

In most cases, the desired output ripple voltage is set to be 2% therefore:

$$C_o \geq \frac{k}{0.02 R f} \tag{1.20}$$

1.9 Conclusion

In this chapter, we have covered the fundamentals of photovoltaic (PV) systems, including their primary types and essential components. We explained the operating principle of solar cells, along with their modeling, evaluation parameters, and characteristic curves. Additionally, we addressed the partial shading phenomenon and its detrimental effects on PV systems. We discussed how bypass diodes can protect PV panels and how this solution can alter the IV and PV curves. The chapter concluded with an overview of DC-DC converters, providing guidelines for designing and selecting their components to ensure efficient and stable operation.

CHAPTER 2 : Maximum Power point tracking techniques

2.1 Introduction

Meteorological circumstances significantly affect the performance of photovoltaic cell. Fluctuations in irradiance, temperature, and the load characteristics may affect the maximum power that can be extracted from the PV system. Partial shading phenomenon is the most significant factor in power losses. To minimize the effect of these challenges, ensuring that the PV system is supplying the maximum possible power for a given weather condition is important. Therefore, maximum power point tracking (MPPT) plays an important role in this process [7].

2.2 Classical MPPT techniques

The hill-climbing method principle provides the foundation for the most common classical algorithms implemented to track the MPP. These strategies are recognized due to being simple to develop and operating well under uniform irradiation. The aim is to adjust the PV array's operating point in the direction of increasing power [8]. We will give a brief summary of the advantages and disadvantages of the two most commonly employed traditional MPPT techniques in this section.

2.2.1 Perturb and observe (P&O) technique

One of the most desirable option for tracking the MPP is P&O, due to simplicity and ease of construction as it require only voltage and current sensor.

- Principle of operation:

The P&O try to locate the MPP by varying the duty cycle sent to the DC-DC converter, which alter the operating voltage according to the power output of the PV array [9]. This perturbation is determined by comparing the previous obtained power with the current one. If the power increase, the algorithm keep perturbing in the same direction. Whenever the measured power decrease, the perturbation will change direction and reduce it value. After repeating this cycle of oscillating around the same operating point a certain amount of iterations with no major change in power, this MPPT method will eventually reach the maximum power operating point. The flowchart in Figure 2.1 is provided below.

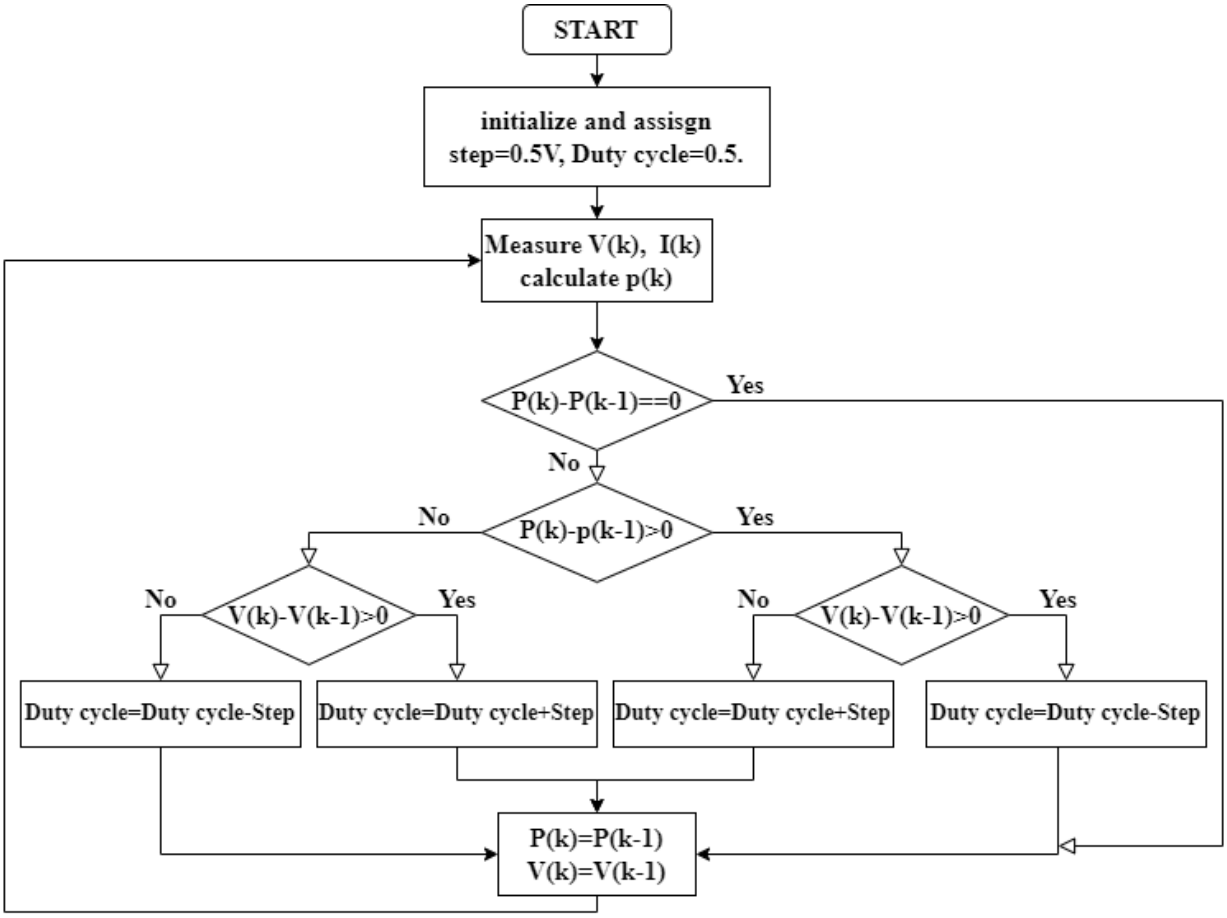

Figure 2.1: P&O based MPPT.

2.2.2 Incremental conductance (IC) technique

The theory behind the incremental conductance method [10-11] (IC) is to determine the terminal voltage of the PV module by measuring and comparing the incremental and instantaneous conductance of the PV module. If it is observed that the incremental conductance is equal to the instantaneous conductance, it indicates that the maximum power point is found, that is:

$$\frac{\partial P_{PV}}{\partial V_{PV}} = V_{PV} \times \frac{\partial I_{PV}}{\partial V_{PV}} + I_{PV} = 0 \qquad (2.1)$$

Equation (2.1) can be reformed as follows

$$\frac{\partial I_{PV}}{\partial V_{PV}} = -\frac{I_{PV}}{V_{PV}} \approx \frac{\Delta I}{\Delta V} \qquad (2.2)$$

Where ΔI , ΔV are the increments in the PV panel current and voltage respectively.

The P-V characteristics are then used to create the IC algorithm's driving equations, which may be represented as follows:

$$\begin{cases} \frac{dP}{dV} < 0 \text{ if } \frac{I_{PV}}{V_{PV}} < -\frac{\partial I_{PV}}{\partial V_{PV}} & \text{on the right of MPP} \\ \frac{dP}{dV} = 0 \text{ if } \frac{I_{PV}}{V_{PV}} = -\frac{\partial I_{PV}}{\partial V_{PV}} & \text{at the MPP} \\ \frac{dP}{dV} > 0 \text{ if } \frac{I_{PV}}{V_{PV}} > -\frac{\partial I_{PV}}{\partial V_{PV}} & \text{on left of MPP} \end{cases} \quad (2.3)$$

As can be seen, the instantaneous conductance of the P-V panel is shown by the right side of the equations, while the incremental conductance is represented by the left.

- **Principle of operation**

At the start of the cycle, the IC algorithm senses the voltage and current values. Based on the aforementioned rules, then it compares the instantaneous conductance (**I/V**) to the incremental conductance **(**ΔI/ΔV**)**. The method is depicted in the flowchart in Figure 2.2.

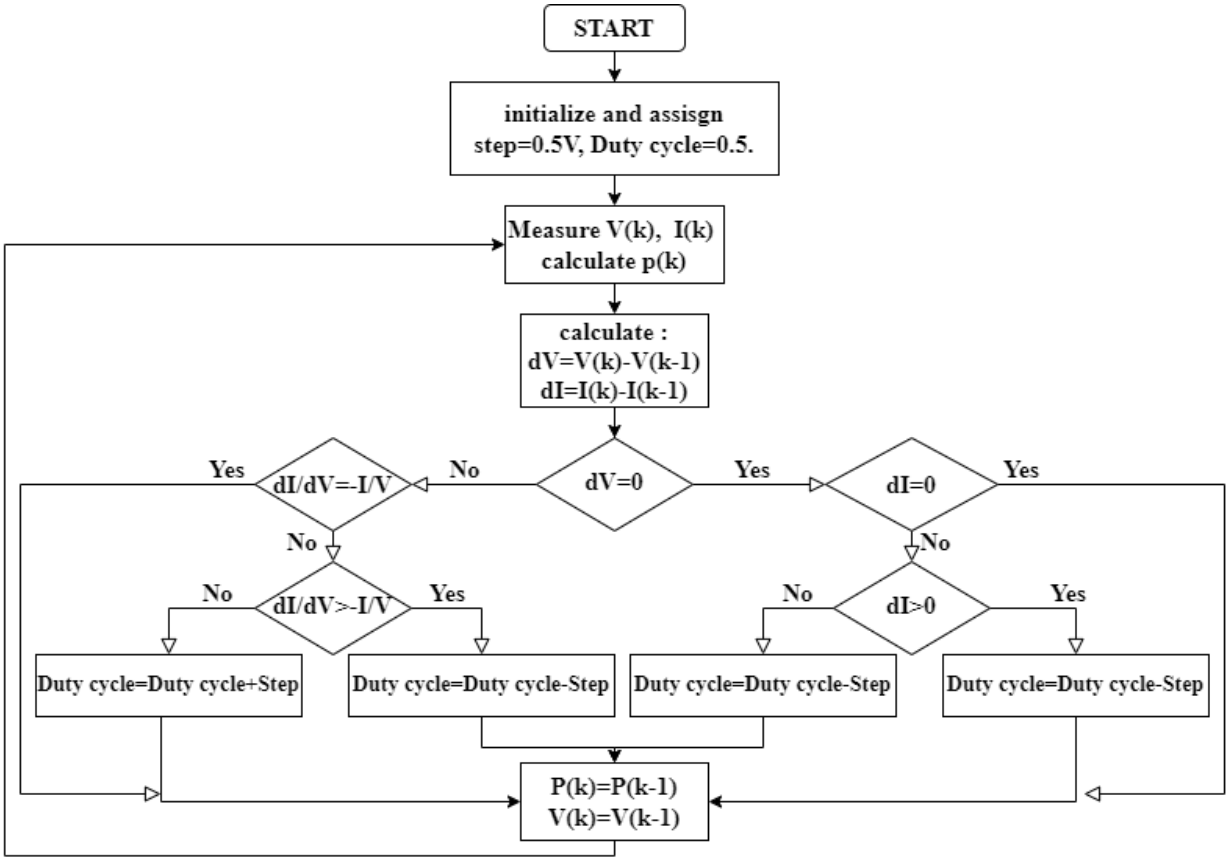

Figure 2.2: IC based MPPT.

2.2.3 Simulation and results

2.2.3.1 Overall system:

To test these two classical methods, a standalone PV system consisting of three modules with a boost converter was designed using Simulink and Matlab. The overall system is shown in Fig 2.3.

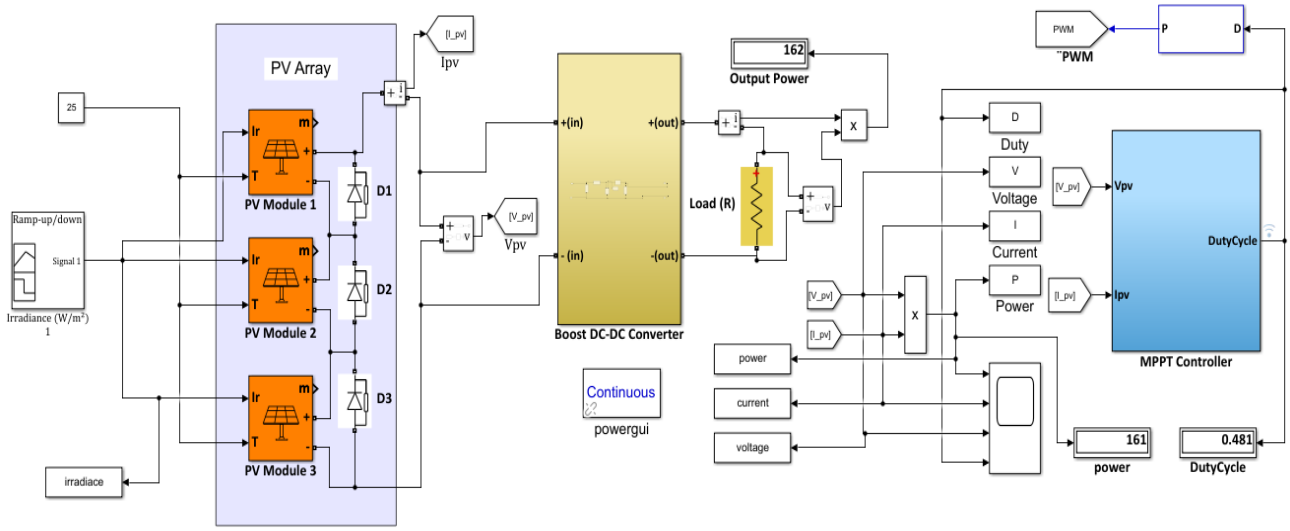

Figure 2.3: Simulink Model of the Designed System

2.2.3.2 PV array Configuration:

The photovoltaic panel model used throughout this work is Soltech 1STH-215-P and has the following characteristics:

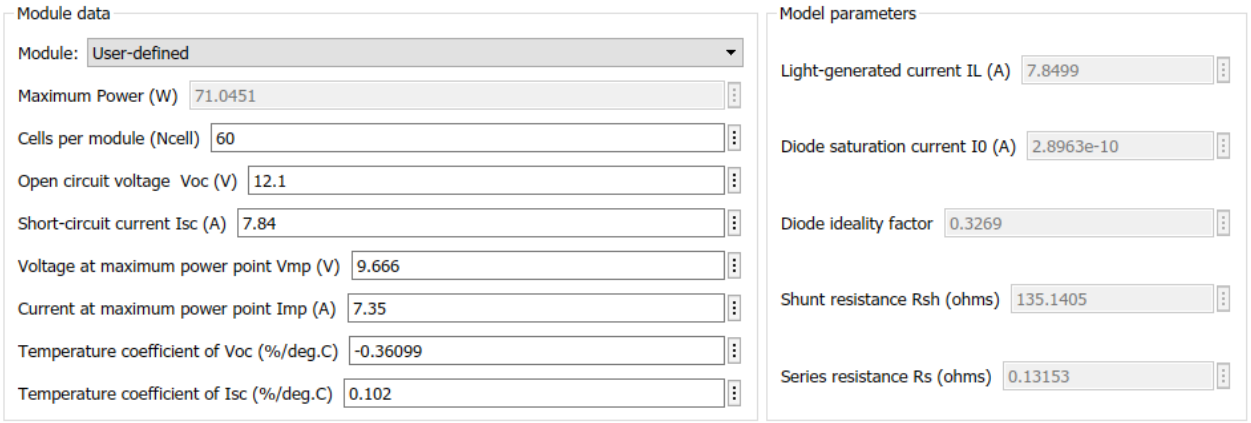

Figure 2.4: Characteristics of the 1Soltech 1STH-215-P PV Panel.

Usually, a standard 60 cell PV module is built from three substrings, of which is protected by a bypass diode [12]. The 3 substrings are serially connected to each other to form a single module.

The P-V characteristics of the used panel under three levels of uniform solar irradiation are depicted in Figure 2.5.

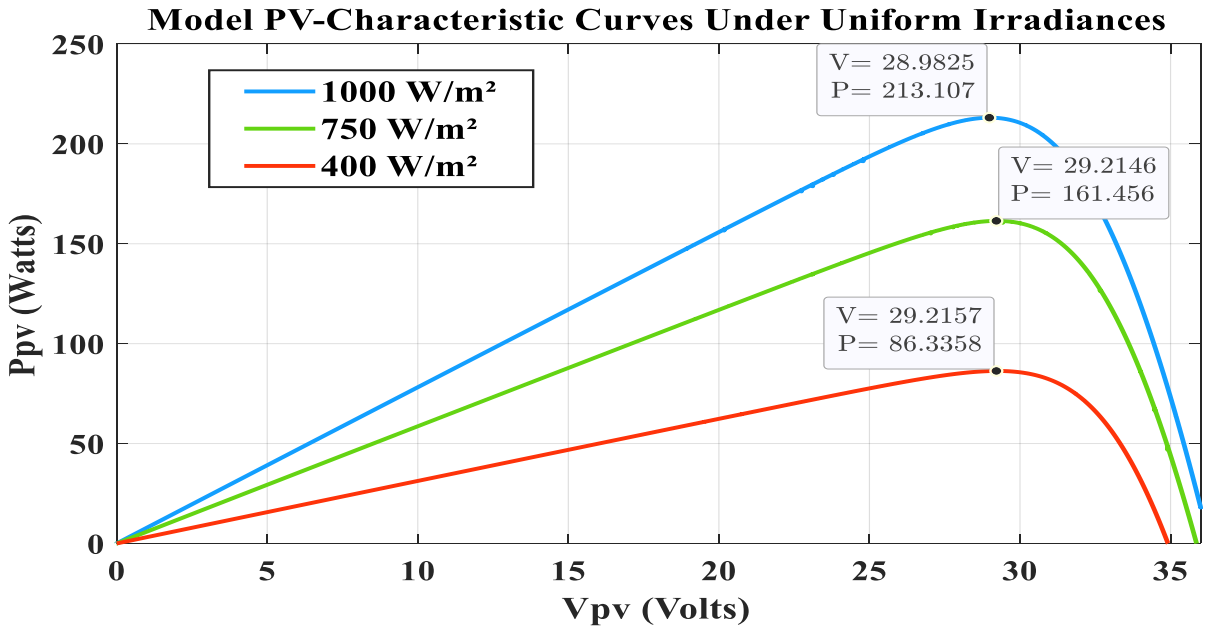

Figure 2.5: The P-V characteristics of the panel under three levels of uniform solar irradiation.

2.2.3.3 DC-DC boost converter design

Setting the switching frequency to be 5 kHz and using the results of Section 1.8, the components of the power converter are provided in Table 2.1.

Table 2.1: DC-DC Converter Components Selection for System 1

Switching Frequency	Inductor (L)	Input Capacitor	Output Capacitor
5 kHz	10 mH	100μF	100μF

2.2.3.4 Simulation:

The PV panel is first exposed to a fast varying uniform solar irradiation of three intensity levels (400, 750, and 1000 W/m²), each of which lasts for 2 seconds. The resulting power, current, and voltage curves of each method are shown in figures 2.6 and 2.7.

a- P&O

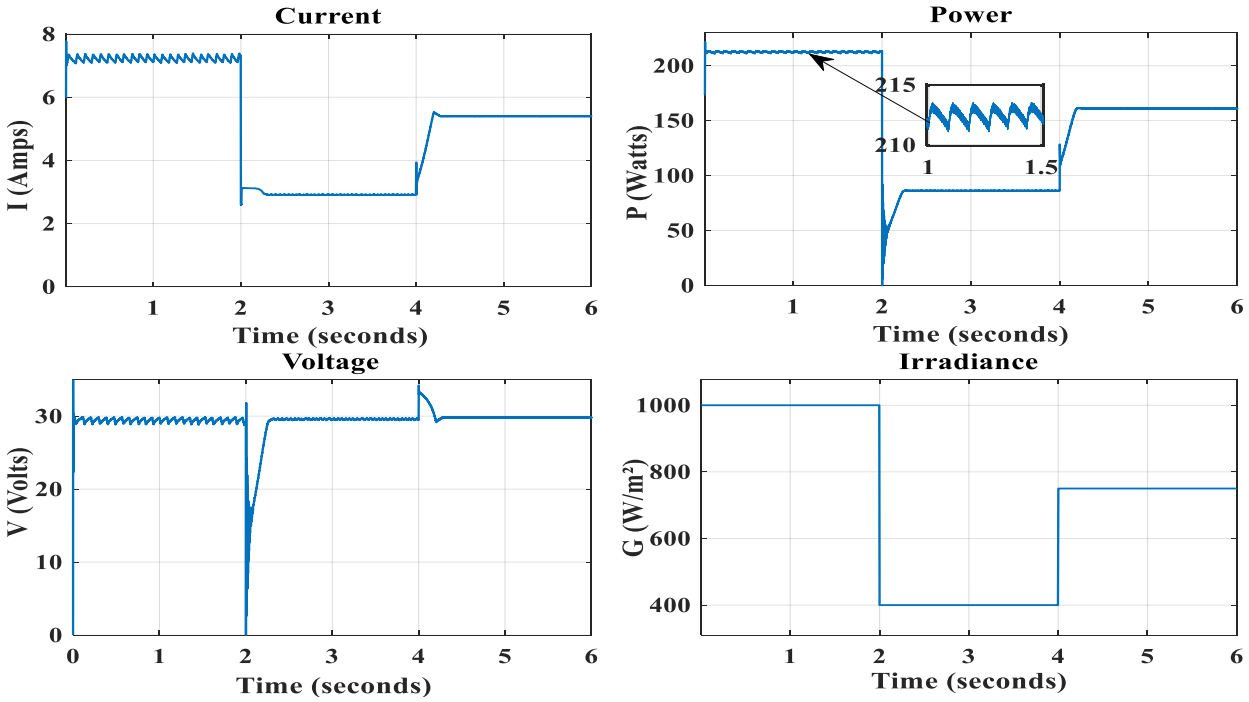

Figure 2.6: Resulting curves under fast varying uniform irradiation using the P&O technique.

b- IC

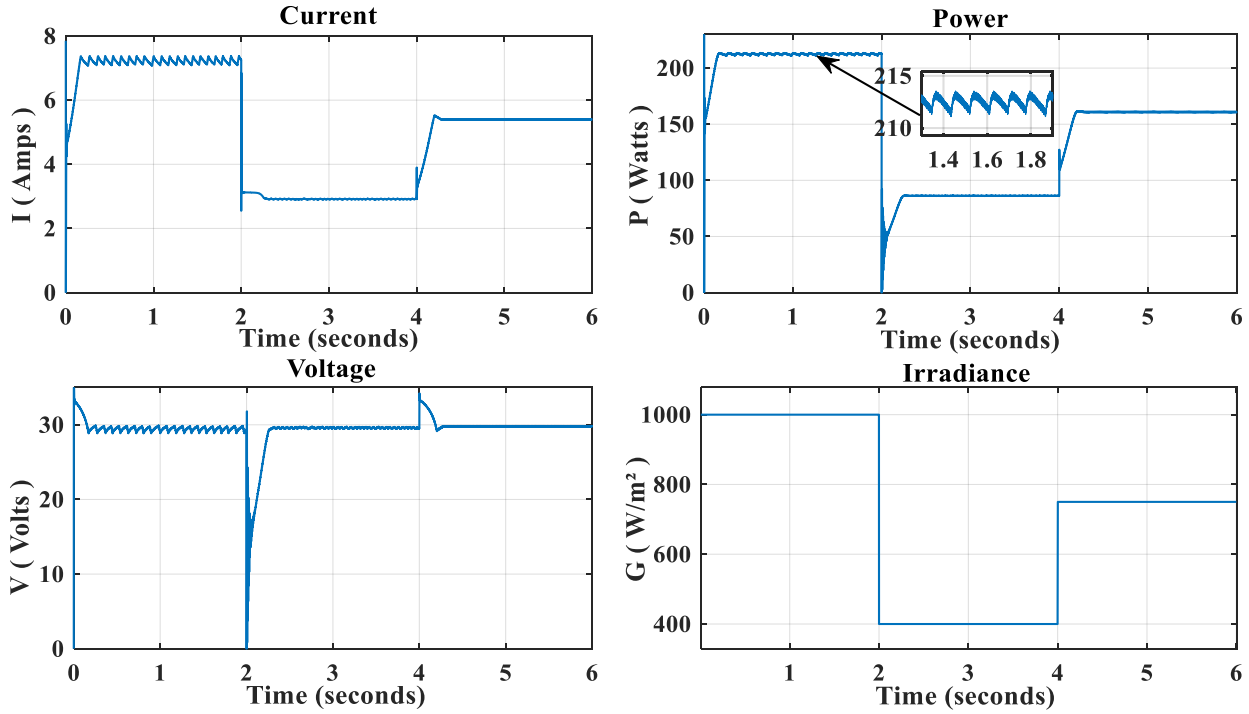

Figure 2.7: Resulting curves under fast varying uniform irradiation using the IC technique.

The system will now undergo partial shading with irradiances of G (500, 750, and 1000 W/m²). The resulting P-V curve consists of three peaks, as shown in figure 2.8.

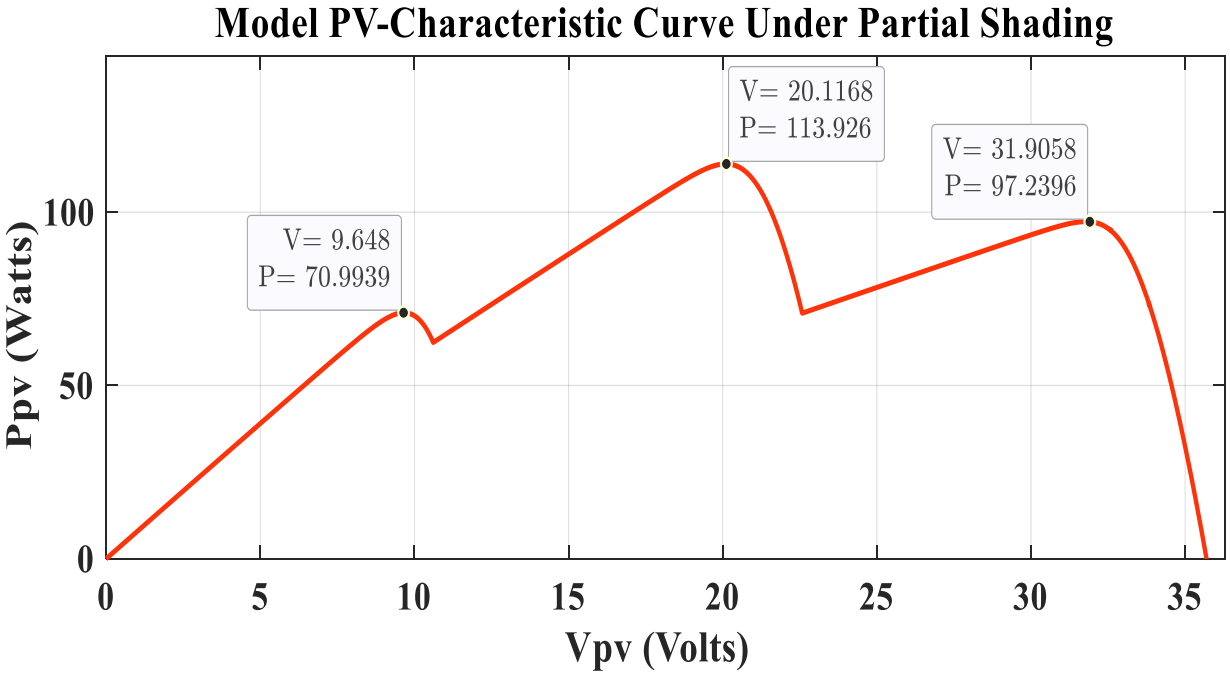

Figure 2.8: Module P-V characteristic curve under partial shading.

a- P&O

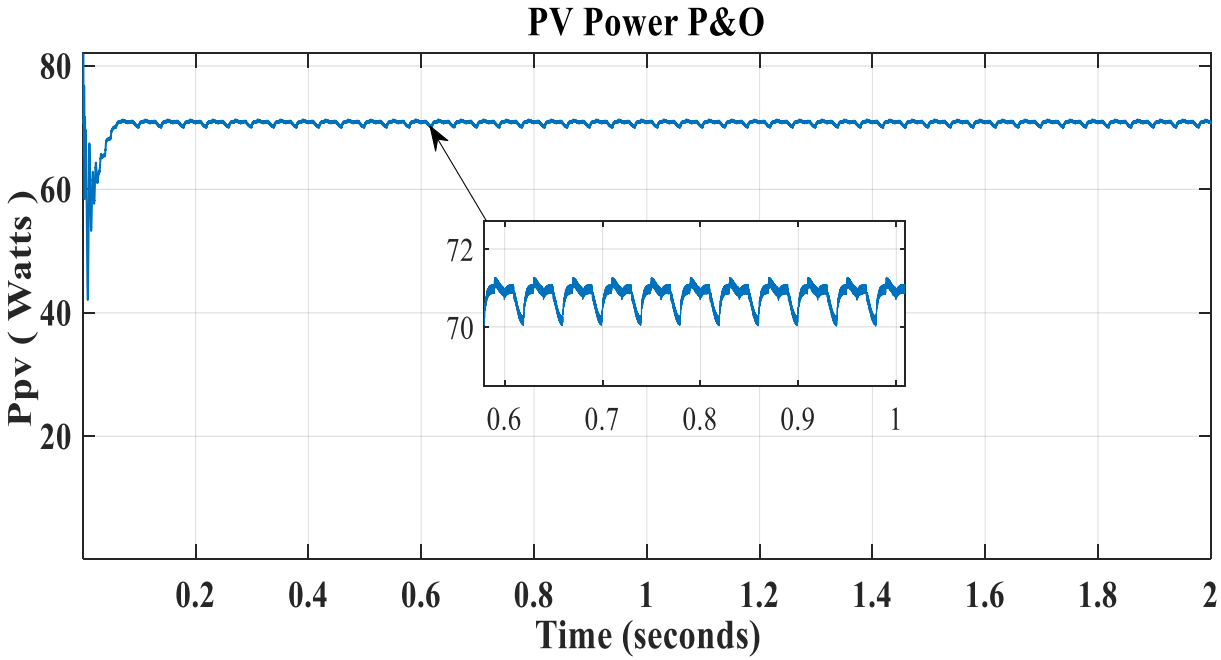

Figure 2.9: Resulting Curves Under Non-Uniform Irradiation Using the P&O Technique.

b- IC

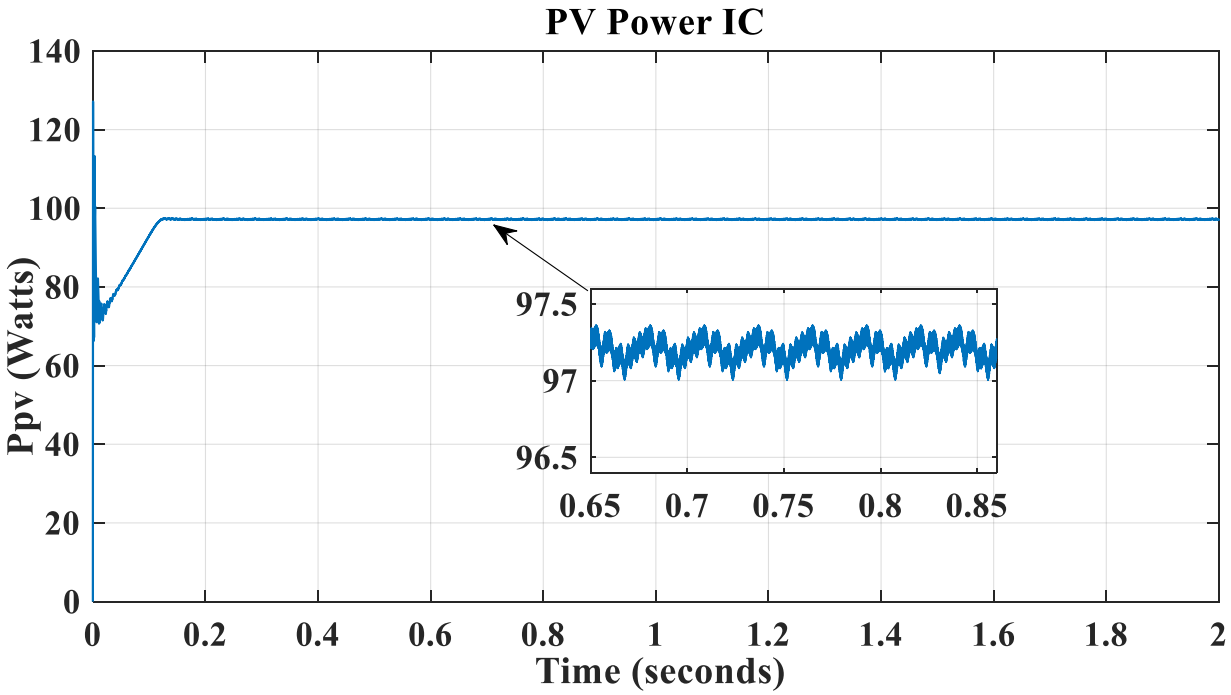

Figure 2.10: Resulting Curves Under Non-Uniform Irradiation Using the IC Technique.

2.2.4 Results and discussion

The simulation results demonstrated two major drawbacks:

- The first drawback is the appearance of oscillation around the MPP, this is due to the fixed step size used at each sampling instant, which forces the operating point to fluctuate around the MPP, thus never reaching an efficient steady state. Controlling the amplitude of these oscillations leads to a fundamental trade-off between tracking accuracy and tracking time. Enhancing the steady state requires a small increment of the reference voltage, thus increasing the convergence duration, and vice versa.
- The second drawback is their ineffectiveness in distinguishing between the global optimum point and the remaining local peaks in partial shading conditions. The two techniques were trapped around the LMPP, which makes them unsuitable in most real life situations.

2.3 Advanced MPPT techniques

Based on section 2.2.4, the previously discussed classical techniques different shortcomings in tracking the MPP most notably, their lack of ability to manage partial shading conditions many soft computing and artificial intelligence algorithms have been developed to solve these obstacles and improve the tracking performance under various conditions. The majority of these alternatives take advantage of metaheuristics, which have demonstrated outstanding results in all operating conditions.

The most popular methods which obtain inspiration from wildlife include those that use genetics, particle swarm optimization, ant colony optimization, whale optimization, grey wolf optimization, and several more. An introduction of two nature-inspired strategies and their most widely used applications [5, 6] are explained alongside MPPT implementations.

2.3.1 Particle Swarm Optimization

Developed by Drs. Eberhart and Kennedy in 1995 [13], particle swarm optimization (PSO) is a population-based stochastic optimization approach that is one of the most widely used algorithms in various optimization engineering issues. It draws inspiration from the social behavior and swarm intelligence of natural species, such as fish schools and bird flocks.

2.3.1.1 Mathematical Modelling and Process Steps

The particle swarm optimization uses a number of population defined as particles that form a swarm wandering around the search space looking for the best solution. Initially, the size of the swarm is defined, and each particle is assigned a random position within the search space to be a candidate solution. The "goodness" of each individual is evaluated by the fitness function related to the optimization problem. In each iteration, the position of each particle is updated based on its personal best location visited so far denoted P_{best} (Personal best solution) and the position of the most successful particle in the whole population denoted by G_{best} (Global best solution).

At the next iteration t+1, the population is updated using the following two equations:

$$x_i^{t+1} = x_i^t + v_i^{t+1} \tag{2.4}$$

$$v_i^{t+1} = \omega v_i^t + C_1 r_1 \left(P_{best,i} - x_i^t\right) + C_2 r_2 (G_{best,i} - x_i^t) \tag{2.5}$$

$$i = 1, 2, \dots\dots\dots, N$$

Where v_i^t and x_i^t are respectively the velocity and position of the ith particle within t iterations, ω is the inertia weight, C_1 and C_2 are the acceleration coefficients, r_1 and r_2 are two generated random numbers that are uniformly distributed in the interval [0, 1].P_{best}, i is the personal best position of particle i achieved so far, and $G_{best}$is the global best position**.** Figure 2.11 depicts the movement of particles in the optimization process.

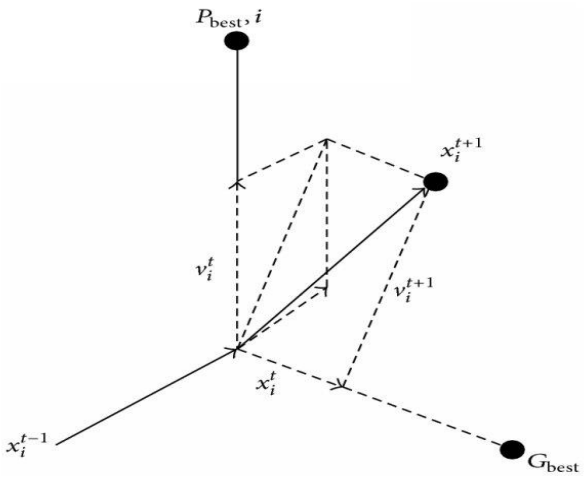

Figure 2.11: Illustration of a Particle's movement during the optimization process [14].

The process of the PSO algorithm can be summarized as follows:

Step1: Initialize the number of particles N_P, maximum number of iterations$T$, $\omega, C_1$and C_2

Step 2: Initialize a population of particles, and randomly assign the location and velocity vectors of each particle.

Step 3: Set iteration t=1.

Step 4: Evaluate the fitness of each particle.

Step 5: Set $P_{best}, i = x_i^t$, and G_{best} to be the particle having the best position.

Step 6: Update the individual's velocities and positions using equations (2.4)-(2.5).

Step 7: Evaluate the fitness of the updated population from step 6, and find the particle having the best position (x_{best}^{t+1}).

Step 8: If the fitness value of the updated i^{th} particle is better than its antecedent fitness, update

$P_{best}, i = x_i^{t+1}$.

Step 9: If the fitness value of the best particle at the current iteration obtained from step 7 is better than the fitness of G_{best}, update $G_{best} = x_{best}^{t+1}$

Step 10: If $t < T$ or the convergence criterion is not fulfilled, then update t=t+1 and repeat steps from 6 to 10, else go to step 11

Step 11: Return the Global best solution G_{best}.

2.3.1.2 PSO based MPPT

In MPPT applications, the objective function is to maximize the output PV power as follows:

$$P(d_i^{t+1}) > P(d_i^t) \tag{2.6}$$

Where $P(d_i^k)$ is the power associated with the i^{th} transmitted duty cycle at the t^{th} iteration.

The PSO technique can be assigned to perform the task of maximum power tracking by initializing a set of N_P several duty cycle options to serve as the positions of particles. The search process will then be carried out as mentioned in the process steps stated above, where G_{best} represents the duty cycle that achieves the largest PV output power. The procedure for tracking the peak power point can be summarized as follows:

Step 1: Initialize the number of duty cycle solutionsN_P, maximum number of iterations T, ω, C_1 and C_2.

Step 2: A solution vector of N_P particles representing a set of duty cycle solutions, and a velocity vector of the same length are initialized.

Step 3: The derived duty cycles are transmitted to the boost converter, and the corresponding PV power is evaluated.

Step 4: Set $P_{best}, i = d_i$ in the first iteration, and obtain G_{best}.

Step 5: Update the duty cycles using equations (2.4) and (2.5).

Step 6: The updated duty cycles are transmitted to the power converter, and the output PV power of each is evaluated.

Step 7: Update P_{best}, i and G_{best}, if better solutions have been obtained.

Step 8: If $t < T$ or the convergence criterion is not fulfilled, iteration is incremented, and steps 5 through 7 are repeated. Else, go to step 9.

Step 9: Transmit the global best duty cycle G_{best} to the power converter.

The algorithm has to be reinitialized whenever a change in weather conditions is detected, according to the following equation:

$$\frac{\left|P_{pv-new} - P_{pv-previous}\right|}{P_{pv-previous}} \geq C \tag{2.7}$$

Where C can be set to 0.1.

The flowchart illustrating PSO-based MPPT is depicted in figure 2.12.

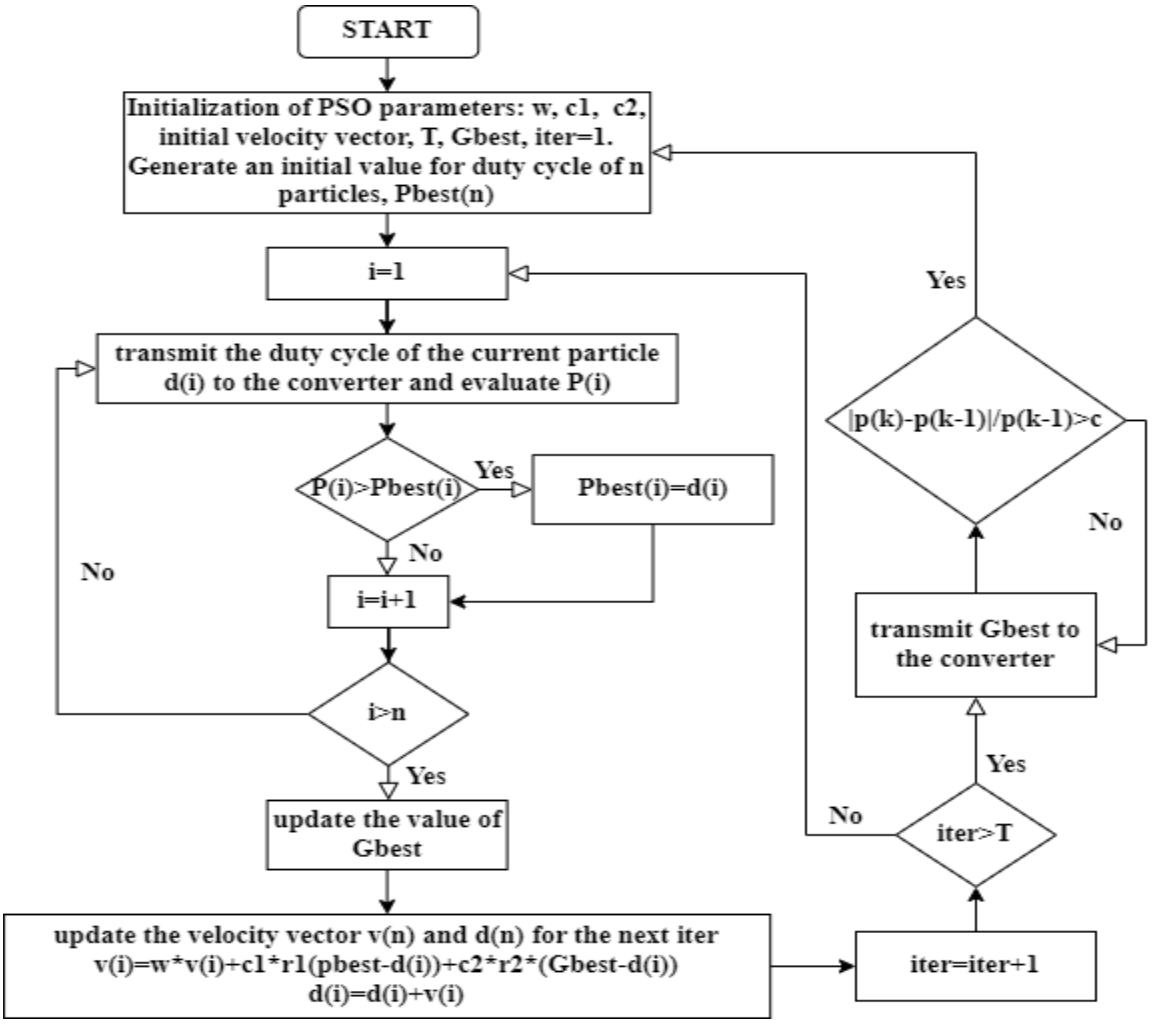

Figure 2.12: PSO-based MPPT.

2.3.2 Grey Wolf Optimization Algorithm

Grey Wolf Optimization (GWO) is a swarm intelligence technique inspired by the hunting behavior and leadership hierarchy of grey wolves in nature [15]**.** In GWO, the pack's members are divided into four groups based on the type of wolf's role that helps in advancing the hunting process [15]: the alphas (α), the betas (β), the deltas (δ), and the omegas (ω), as shown in Fig. 2.13 and 2.14. The alphas are the most powerful and dominant agents in leading the group; the betas represent the secondary wolves that assist the alphas in making decisions, whereas the omegas have the lowest rank. If a wolf is neither an alpha nor a beta, or an omega, it is considered a delta (subordinate). Another behavior of grey wolfs is their appealing group hunting strategy, which consists of a set of phases:

- Tracking, chasing, and approaching the prey.
- Pursuing, encircling, and harassing the prey until it stops moving
- Attacking the prey.

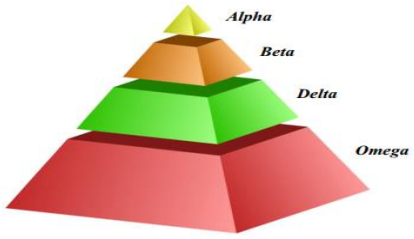

Figure 2.13: Social Hierarchy of Grey Wolves [16].

Figure 2.14: Hunting behavior of grey wolves: (a-c) chasing, approaching and tracking prey; (d) encircling; (e) stationary situation and attack [17].

2.3.2.1 Mathematical Modeling

A - Social hierarchy

In order to mathematically model the social hierarchy of grey wolves, the three best-so-far solutions are considered to be the alpha (α), beta (β), and delta δ) agents, where alpha represents the fittest solution, while beta (β) and delta (δ) are the second and third fittest agents, respectively.

B - Encircling the prey

In order to model the encircling strategy, the following equations are used:

$$\overrightarrow{D} = \left|\overrightarrow{C}.\overrightarrow{X}_p(t) - \overrightarrow{X}(t)\right| \quad (2.8)$$

$$\overrightarrow{X}(t+1) = \overrightarrow{X}_P(t) - \overrightarrow{A}.\overrightarrow{D} \quad (2.9)$$

Where t indicates the current iteration, $\overrightarrow{A}$ and $\overrightarrow{C}$ are coefficient vectors, $\overrightarrow{X}_P$ is the position vector of the prey, and $\overrightarrow{X}$ indicates the individual position vector .The vectors $\overrightarrow{A}$ and $\overrightarrow{C}$. are calculated as follows:

$$\overrightarrow{A} = 2\vec{a}.\overrightarrow{r_1} - \vec{a} \quad (2.10)$$

$$\overrightarrow{C} = 2.\overrightarrow{r_2} \quad (2.11)$$

In Equations (2.10) and (2.11), $\overrightarrow{r_1}$and $\overrightarrow{r_2}$are random vectors in the interval [0,1]. Whereas $\vec{a}$ is a linearly decreased parameter from 2 to 0.

C - Hunting

During the hunting process, the GWO assumes that the alpha, beta, and delta agents are more versed about the promising regions of the prey locations. The search process is then guided by these agents using the following equations:

$$\overrightarrow{D_\alpha} = \left|\overrightarrow{C_1}.\overrightarrow{X_\alpha} - \overrightarrow{X}\right| \quad (2.12)$$

$$\overrightarrow{D_\beta} = \left|\overrightarrow{C_2}.\overrightarrow{X_\beta} - \overrightarrow{X}\right| \quad (2.13)$$

$$\overrightarrow{D_\delta} = \left|\overrightarrow{C_3}.\overrightarrow{X_\delta} - \overrightarrow{X}\right| \quad (2.14)$$

$$\overrightarrow{X_1} = \overrightarrow{X_\alpha} - \overrightarrow{A_1}.(\overrightarrow{D_\alpha}) \quad (2.15)$$

$$\overrightarrow{X_2} = \overrightarrow{X_\beta} - \overrightarrow{A_2}.(\overrightarrow{D_\beta}) \quad (2.16)$$

$$\overrightarrow{X_3} = \overrightarrow{X_\delta} - \overrightarrow{A_3}.(\overrightarrow{D_\delta}) \quad (2.17)$$

$$\overrightarrow{X}(t+1) = \frac{(\overrightarrow{X_1} + \overrightarrow{X_2} + \overrightarrow{X_3})}{3} \quad (2.18)$$

Where $\overrightarrow{X_\alpha}$, $\overrightarrow{X_\beta}$ and $\overrightarrow{X_\delta}$ indicates the position vector of the alpha, beta, and delta agents respectively, Figure 2.15 demonstrates how a search agent updates its position according to alpha, beta, and delta in a 2D search space. It can be observed that the final position would be in a random place within a circle, which is defined by$\overrightarrow{X_\alpha}$, $\overrightarrow{X_\beta}$, $\overrightarrow{X_\delta}$ in the search space. In other words, alpha, beta, and delta estimate the position of the prey, and other wolves update their positions randomly around the prey [18].

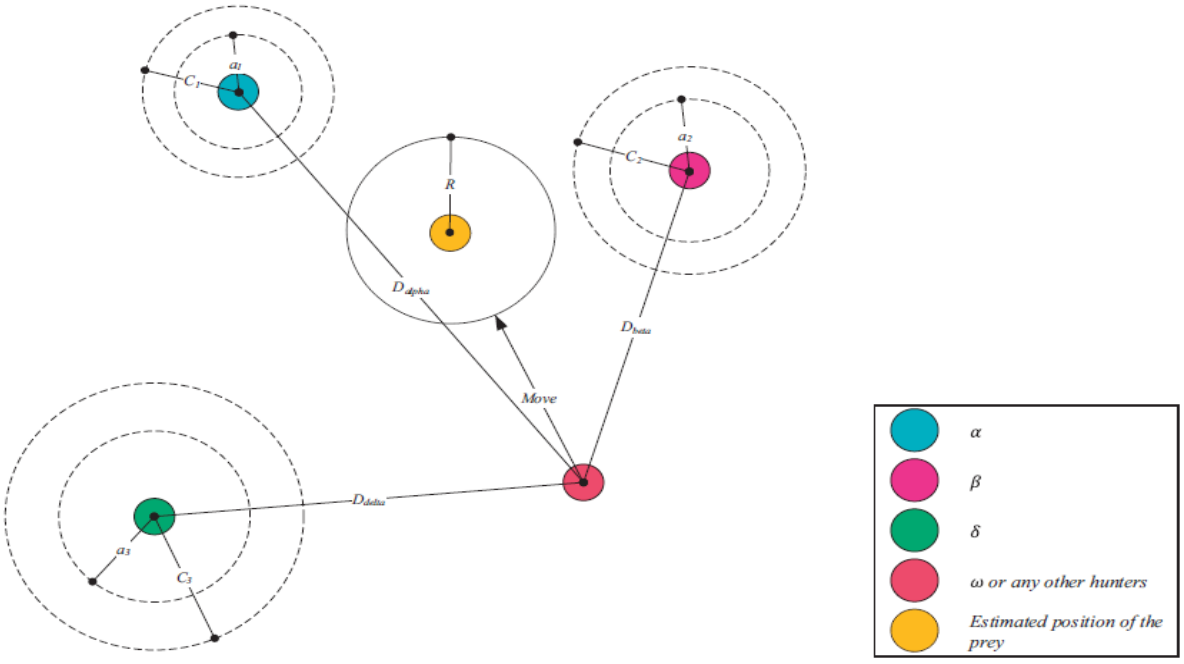

Figure 2.15: Position Updating in GWO.

2.3.2.2 Exploration and Exploitation

The parameters A and C are the main factors that determine the balance between exploration and exploitation.

With A decreasing throughout the optimization process (since a is linearly reduced over [0,2]), half of the iterations are dedicated to exploration *(*$|A| \geq 1$), whereas the others are devoted to exploitation ($|A| < 1$). The C vector contains random values in [0, 2]. This component provides random weights for the prey in order to stochastically emphasize C >1 or deemphasize C <1's

Effect in defining the distance in Eq. (2.9). This assists GWO to exhibit more random behavior during optimization, favoring exploration and local optima avoidance [19]. The pseudo code of the GWO algorithm is given below:

Algorithm 1 Grey Wolf Optimization

Initialize the grey wolf population X_i $(i = 1, 2, \ldots, n)$
Initialize A, a and C
Calculate the fitness of each search agent
$X_\alpha \leftarrow$ the best search agent
$X_\beta \leftarrow$ the second best search agent
$X_\delta \leftarrow$ the third best search agent
while $t <$ max number of iterations do
    for each search agent do
        Update the position of the current search agent by equation (2.18)
    end for
    Update a, A and C
    Calculate the fitness of all search agents
    Update X_α, X_β and X_δ
    $t \leftarrow t + 1$
end while
return X_α

2.3.2.3 GWO based MPPT

The flowchart illustrating the Grey Wolf Optimization based MPP tracker is shown in Figure 2.16:

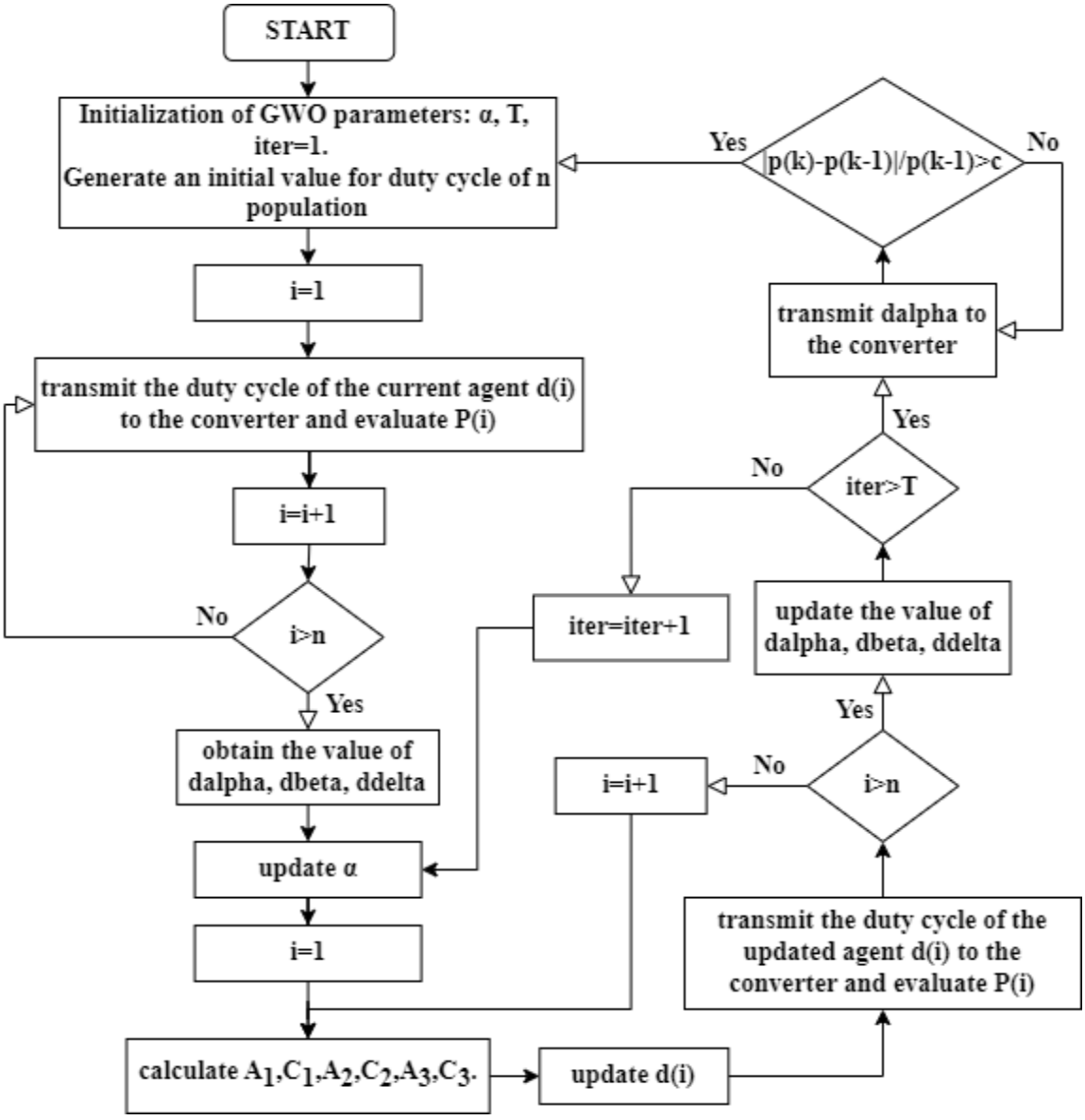

Figure 2.16: GWO-based MPPT

2.4 Proposed algorithm

2.4.1 Inspiration

This method is an Enhanced Adaptive P&O MPPT, which draws inspiration from PSO's ability to locate the GMPP region under partial shading conditions while using adaptive P&O, followed by

evaluating the peak with a Lagrangian interpolation formula for fast convergence to the MPP in that region.

Recently, there have been efforts to combine the P&O with metaheuristic algorithms such as FF, ACO, PSO, and GW to track the global peak under partial shading. This is known as the hybrid approach [20], [21], and [22]. Unfortunately, by doing so, the P&O loses its simple structure. Furthermore, the computational burden has significantly increased due to the incorporation of metaheuristic algorithms.

The objective of this work is to propose an enhanced adaptive P&O (EA-P&O) that minimizes steady-state oscillation, similar to the work carried out in [23]. In addition, the algorithm detects the partial shading occurrence and performs a rapid search for the global peak. Another important feature is that the values of open circuit voltage and irradiance are continuously updated without the use of irradiance sensor. This reduces the cost and complexity of the MPPT implementation considerably.

2.4.2 WORTHWHILE I–V CHARACTERISTICS OF SHADED PV ARRAYS

Partial shading often occurs due to shadows created by passing clouds, the presence of snow, trees, and nearby objects. The shaded cells could become reverse biased, acting as a load and dissipating power from the irradiated cells [24]. The PV manufacturers and installers normally use bypass diodes to prevent hot-spot problems and to stop unproductive cells from disrupting the production of active cells. The resultant PV characteristics of the shaded PV array introduce new challenges for the control of power electronic interfaces to optimize energy harvesting.

Fig.2.17 (a) and (b) depict the P-V graph and I-V graph, respectively, of a partially shaded Soltech 1STH-215-P PV module, which includes three bypass diodes. The P-V graph exhibits three power peaks as a result of three different irradiance levels on the PV module. In practice, the PV modules are assembled in parallel-series configuration to form a PV array in order to provide the expected power. This configuration is not fixed for a certain level of power, and the PV developers design the PV array for specific objectives. The number of power peaks appearing in the P-V graph depends on the configuration of the partially shaded PV array and the shading pattern. Moreover, the location and magnitude of the power peaks are greatly variable due to the variety of possible PSCs.

On the other hand, the I-V graph of a partially shaded PV array represents a simpler characteristic. Some simple observations that are true for any PV array configuration under different PSCs are presented as follows:

1) The I-V graph exhibits several steps. The current magnitude increases when sweeping the I-V graph from open-circuit voltage toward the short-circuit voltage, no matter the partial shading pattern or PV array configuration, as can be seen in Fig. 2.17(b).
2) In each step, the operation of the PV array could be categorized into two stages: (1) the left-hand side of the MPP (LHS-MPP) and (2) the right-hand side of the MPP (RHS-MPP). In the LHS-MPP, the PV characteristic experiences a very small variation in current level. Hence, if the PV system works on the MPP of a step, a small perturbation in the current level would force the operating point to the RHS-MPP of the next step.
3) In the RHS-MPP, the voltage range is small. Thus, if the operating point happens to be in this range, the MPP of this step could be reached quickly with a small decrease in PV array voltage.

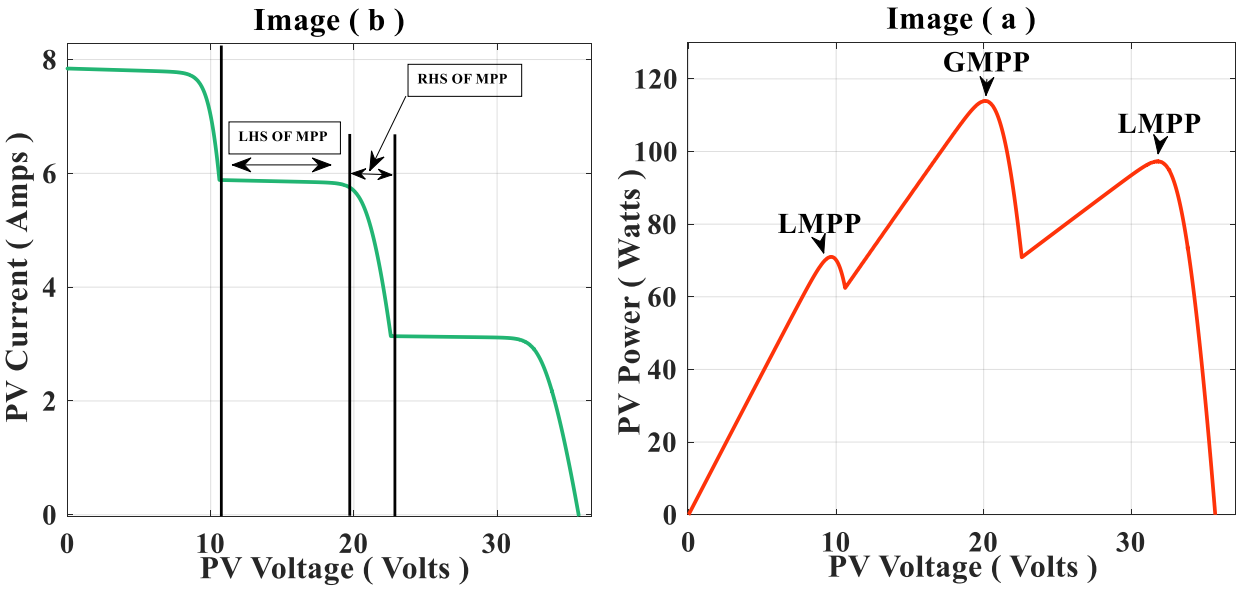

Figure 2.17: I–V and P–V Characteristics curves during non-uniform irradiance

These observations could be easily realized from any I–V graph of partially shaded PV arrays. They are not dependent on the PV module arrangement within the PV array, datasheet information of PV module manufacturer, shading pattern, or ambient condition.

2.4.3 EA-P&O based MPPT

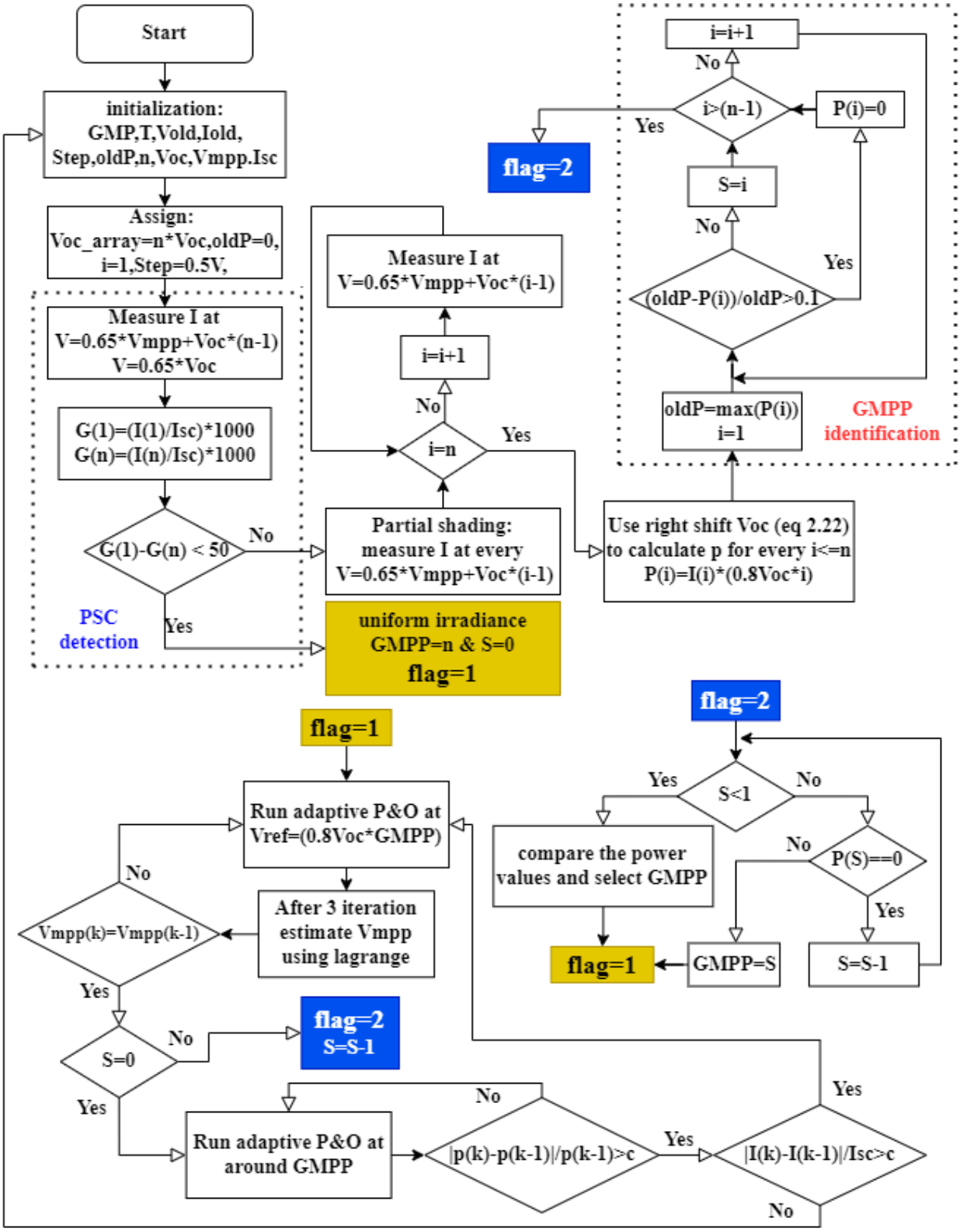

Figure 2.18: Flowchart for EA-P&O

2.4.3.1 Initialization

The objective of the EA-P&O is to ensure that steady state oscillation along with the tracking of the global peak under partial shading. To accomplish that, the complete flowchart is implemented as illustrated in Fig. 2.18. EA-P&O requires several initialization parameters as given in Figure 2.4. To facilitate numerical explanation, data from Soltech 1STH-215-P PV module has been presented in Figure 2.4.

2.4.3.2 Tracking under Uniform Irradiance

Based on critical observation by numerous researches [25], [26] that the MPP lies in the vicinity of 0.8 × V_{OC} array (V_{OC} array = V_{OC} × N). It is explained in [23] that, it is appropriate to initialize at 0.65 × V_{OC} array, so that MPPT can record few perturbation directions before converging at indicated voltage. It is presented in [27], [28], majority of the MPPT algorithm in literature cannot distinguish between sudden change in irradiance or partial shading. Whenever, they sense a large change in power they initiate global peak searching under partial shading although partial shading may not be present at that time.

However, EA-P&O initiate two specific voltage on the curve at $V_1 = 0.65V_{OC}$ and $V_2 = 0.65V_{MPP} + 0.8V_{OC}*(N-1)$. Here, V_1 and V_2 lies close to short circuit current position. Thus, recorded current at these two points are I_1 and I_2 represents ISC. Afterwards, based on these two-current values irradiance level (G) on the I-V curve can be calculated as follows [27].

At $V_1 = 0.65V_{OC}$

$$G_1 = \frac{I_1}{I_{SC-STC}} * G_{STC} \tag{2.19}$$

At $V_2 = 0.65V_{MPP} + 0.8V_{OC}*(N-1)$

$$G_2 = \frac{I_2}{I_{SC-STC}} * G_{STC} \tag{2.20}$$

This proposed scheme can be numerically verified using the following example. In Fig. 2.19, I-V curve under three irradiance level (1000, 600 and 300 W/m2) is illustrated. On the curve, respective currents for the $I_1 = I_{0.65VOC}$ and $I_2 = I_{0.65VMPP+0.8VOC*(N-1)}$ are marked. For Soltech 1STH-215-P PV module at STC the I_{SC} is 7.84 A. At 1000 W/m^2, using (2.19) & (2.20) the G1 and G2 can be calculated as follows:

At V_1=7.87

$$G_1 = \frac{I_1}{I_{sc-STC}} * G_{STC} = \frac{7.82}{7.84} \times 1000 = 998.7\ \mathrm{W}/m^2$$

At V_2=25.64

$$G_2 = \frac{I_2}{I_{SC-STC}} * G_{STC} = \frac{7.72}{7.84} \times 1000 = 984.7\ \mathrm{W}/m^2$$

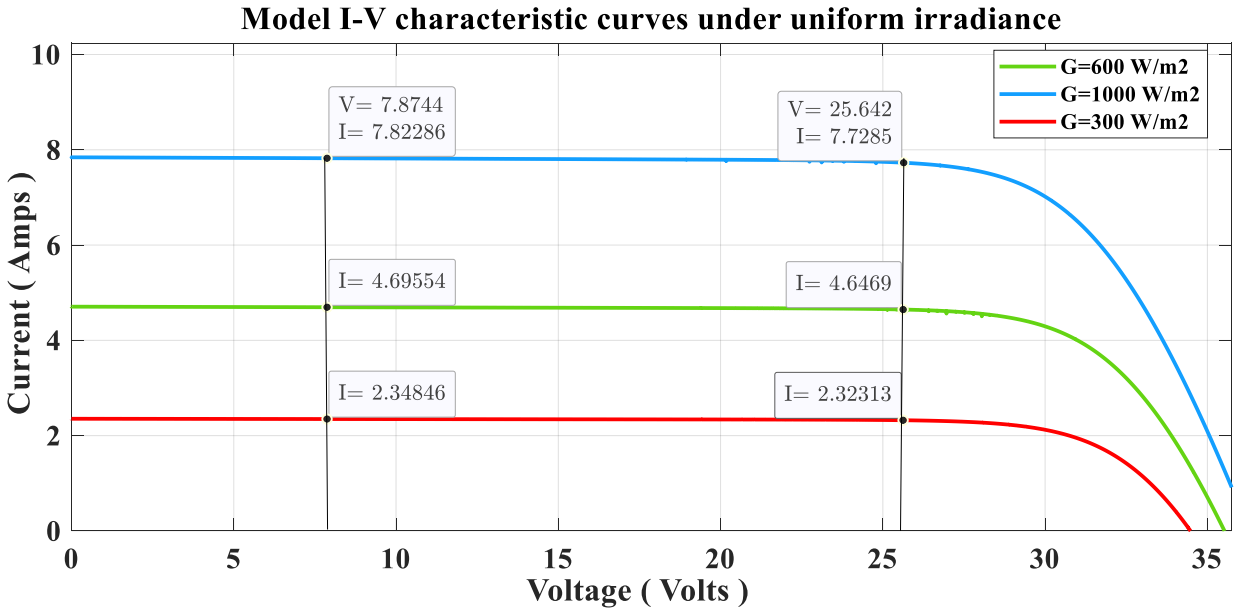

Figure 2.19: Characteristics of I-V curve during uniform irradiance

It can be seen that the calculated values of G1 and G2 are very close to the actual 1000 W/m^2. However, values differ by 14.

Similarly using the I-V curve for 600 W/m2, the values of G1 and G2 is 592.7 W/m^2 and 599 W/m^2, thus having mismatch of 6.2. However, it is noticeable that, at 300 W/m2 the calculated value for G1 is 296.3 W/m2 but G2 is 299.5 W/m2 which has a discrepancy of 3.2. Based on these observations, an important deduction can be made: once G1 and G2 is calculated and mismatch remains below a certain threshold, the algorithm treats the condition as a uniform irradiance.

It is reported in [27] that, in mono and poly crystalline based PV modules the absolute difference between G1 and G2 always remain less than 40 under uniform irradiance. Thus in Fig. 2.18, a checking is done to find the difference between G1 and G2. Though instead of 40, threshold is set to 50 to have a margin of safety. If a large power deviation is due to large change of uniform

irradiance, then |G1 − G2 | will remain below 50, otherwise it will be considered as a partial shading case.

Then, it initiates P&O under flag 1 and tracks the MPP precisely along with minimizing perturbation size. To notify uniform irradiance condition or distinct GMP, a variable named 'S' is assigned as 0. On the contrary, if it is a case of partial shading then variable 'S' is assigned a value according to the region, that suspected to be the GMP region. Then EA-P&O initiate flag 2 (in Fig. 2.18) where it performs global peak searching under partial shading.

2.4.3.3 Scanning Under Partial Shading

Under partial shading, the local peaks occur at some specific points. According to 0.8Voc model [25], [26] local peaks are expected at the vicinity of the multiples of $0.8V_{OC}$. Thus, scanning the voltages, located at every ($0.65V_{MPP}$ + (i^{th} -1) × $0.8V_{OC}$) to record the measured current I at each region i, provide an estimation of the current at the LPP. Then find the global peak by comparing predicted power at every multiple of $0.8V_{OC}$ is very straight forward:

$$P_{LMP}(n) = I_n * n * (0.8 * V_{OC}) \quad (2.21)$$

However, it is presented in [29] that when shading level increased along with the number of modules in series, the local peak's positions shifted towards right on the voltage span and the deviation from the multiples of 0.8Voc is significant. Thus, to improve the accuracy, it is important to right shift the predicted points along with the increase of the shading level. So, an improved estimation technique is developed and integrated with EA-P&O.

To describe the procedure, the curve presented in the Fig. 2.20 is considered. The number of modules in series is 9 and these are irradiated by 1000, 750, 500 and 300 W/m^2. The number of modules under each irradiance levels are 3, 2, 2 and 2 respectively. In Fig. 2.20, samples taken by the $0.8V_{OC}$ model is presented. It can be seen if the points according to the $0.8V_{OC}$ model is scanned, the 3^{rd} point is at the LMPP1. However, the 5^{th} is not coinciding with the LMPP2. In the other hand 8^{th} passed the LMPP3, and LMPP4 is far from the 9^{th} point. This is happening due to the right shifting of the peaks, As a result each region's LMPPP is estimated incorrectly.

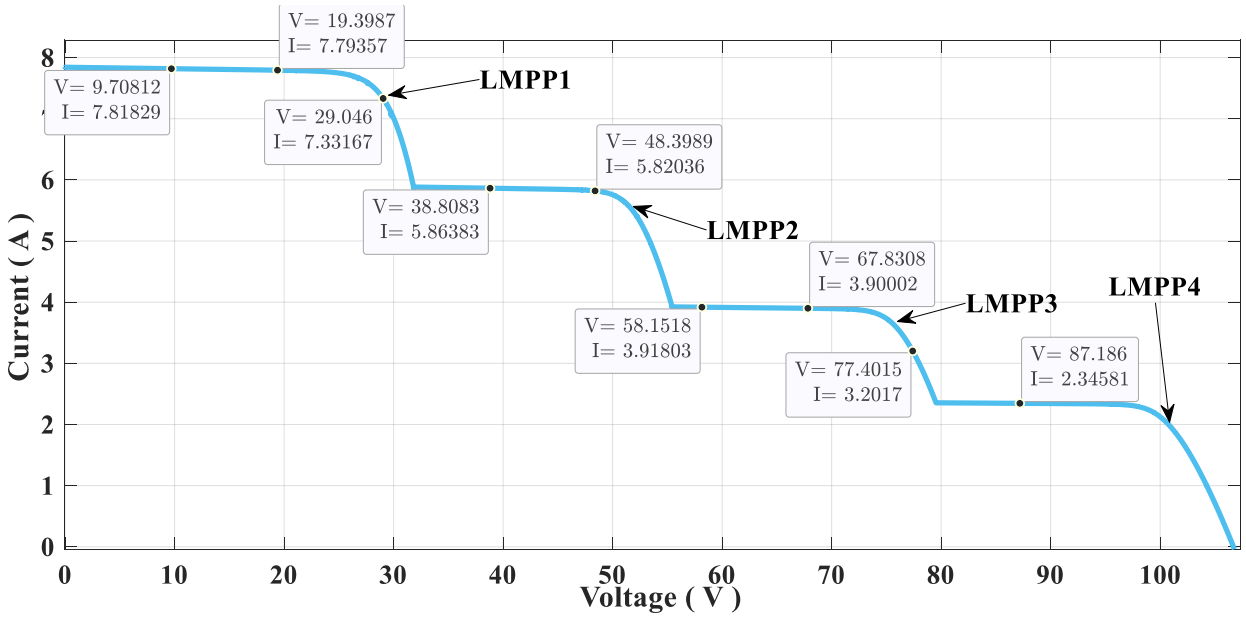

Figure 2.20: I-V Characteristic Curve of Predicted points by 0.8Voc model

In Fig. 2.21, V_{LPPs} occurs at the 0.8Voc points by assigning [V_{LPP1}, V_{LPP2}….$V_{LPPN\ s}$] = [0.8 × 1 × V_{OC}, 0.8 × 2 × V_{OC}.....0.8 × Ns × V_{OC}] initially. The first point (V1, I1) is near to the short circuit current. The current is used to calculate the G at the first stair of the current using (2.19) which is 1000 W/m^2. Then, it measure point V2 and records current I2. If G is calculated using (2.20) at I2, then the irradiance level is found almost near (difference is less than 50) to the calculated G at I1. Same observation goes for I3. However, when (V4, I4) is measured and G is calculated as (5.864/7.84 = 747.96 W/m^2), EA-P&O realize that current level falls to the second stair. As a consequence, the rest of the predicted peak points needs to be shifted right. Using the proposition in [29], local peak position can be calculated considering right shifting phenomenon as follows.

$$V_n = \left[0.8 + (0.97 - 0.8) * \frac{1000}{900} * \frac{(I_1 - I_n)}{I_{SC_{STC}}} \right] * n * V_{OC} \qquad (2.22)$$

According to

$$V_4 = \left[0.8 + (0.97 - 0.8) * \frac{1000}{900} * \frac{(I_1 - I_4)}{I_{SC_{STC}}} \right] * V_{OC} * 4 = 40.99\ V$$

Due to the right shifting V4 is shifted to 41 V instead of 38.7 V (0.8Voc model) Thus, the V5 is also shifted to 51.31 V which is at the LMPP2 precisely. At V6 EA-P&O sense a change of irradiance level and shift the rest of the peaks including V6 according to (2.22).

As a result, V7 is coinciding within the LMPP3 accurately. The similar phenomenon will again take place at V8 (88.2) V and shift the V8 and V9 to 90.2 V and 101 V respectively. V9 is the actual location of LMPP4 as marked on Fig. 2.21. The conclusion can be drawn as the right shifting mechanism is implemented, the prediction regarding the local peaks position gets more accurate. After sampling all regions and correctly predicting it peaks location, the expected power will be compared based on the values of measured current and calculated V_{LMPP}, then the highest power providing position will be considered as the global peak.

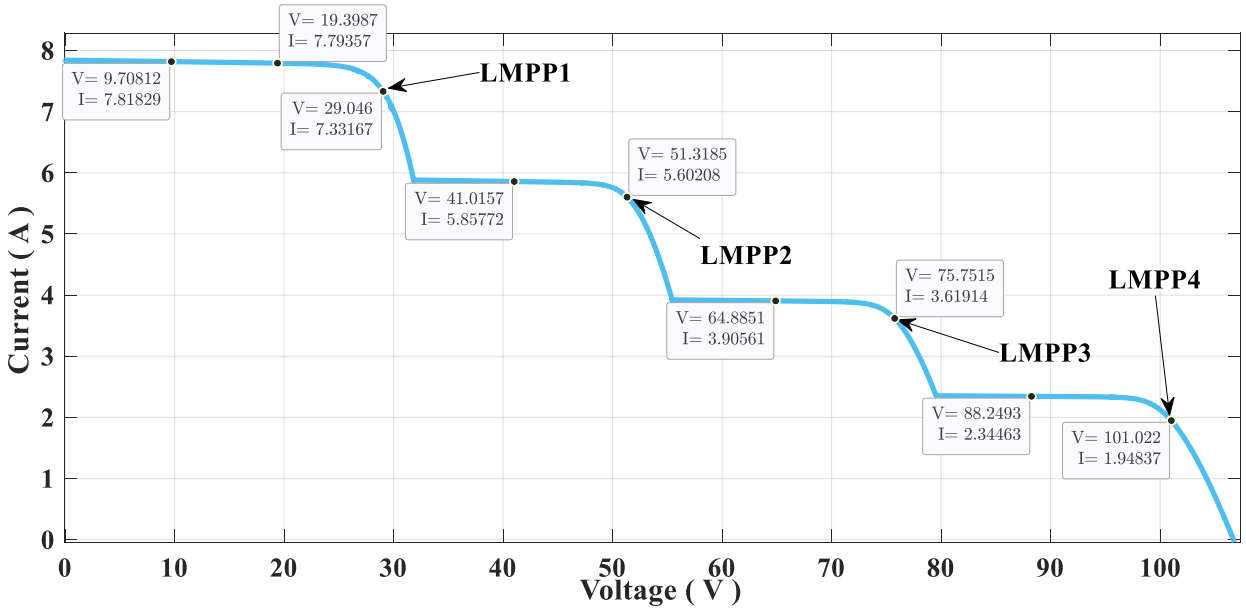

Figure 2.21: I-V Characteristic Curve of Predicted points by EA-P&O

Like all other semiconductor devices, solar PV cells are sensitive to temperature. With the increase in temperature, the band gap energy of semiconductor material gets reduced, so the current increases slightly but the voltage decreases significantly. Therefore, the energy conversion efficiency of silicon solar cell reduces about 0.3% when its temperature increases by 1°C [30, 31].

When attempting to predict the precise LMP, it becomes more challenging to account for the variation of each PV panel's V_{OC} due to ambient temperature fluctuation. As a solution, permitting a margin of uncertainty provides an approach to distinguishing between a GMPP and an LMP that

differ by no more than 10% in output expected power. As a result, EA-P&O discards any region that doesn't meet the 10% margin of error criteria after estimating every LMP. Narrowing the scope of searching to just those regions that might include GMPP increases the probability that GMPP is found.

2.4.3.4 Adaptive Lagrange based P&O

Unlike conventional techniques, where perturbing and observing power are used to track the PV MPP resulting in long computations time, the proposed algorithm computes the value of initial D_{MPP} (duty cycle at MPP) based on the voltage at maximum power. Therefore, the algorithm can start the optimization process with an initial value that is already close to the GMPP.

The algorithm begins by obtaining the present value of V (k) and using the previous value, stored at the end of the preceding iteration, V (k-1). Then the value of the next V (k+1) is estimated, using adaptive P&O as flow [32]:

$$V_{k+1} = V_K + \frac{(P_K - P_{K-1})}{(V_K - V_{K-1})} \tag{2.23}$$

Where ΔP and ΔV represent the changing power and voltage respectively. This setting is to make sure that the step will be large enough to cope with the rapid change of either irradiation or cell temperature, and gradually reduced down to zero when the system reaches GMPP.

After three iteration, The algorithm switch to using the Lagrangian interpolation formula, for which four points obtained previously from the (I-V) characteristic are used. The value of the duty cycle at MPP D_{MPP} at (V_{MPP}) can be estimated using the Lagrangian interpolation formula, which is described by a quadratic interpolation function. Eq (2.24) below gives the interpolation formula for power P corresponding to voltage V [33]:

$$P(V) = \frac{(V - V_{K-1})(V - V_{K-2})(V - V_{K-3})}{(V_K - V_{K-1})(V_K - V_{K-2})(V_K - V_{K-3})} P_K + \ldots + \frac{(V - V_K)(V - V_{K-1})(V - V_{K-2})}{(V_{K-3} - V_K)(V_{K-3} - V_{K-1})(V_{K-3} - V_{K-2})} P_{K-3} \tag{2.24}$$

This optimization approach will help overcome the problem posed by P&O method which is slow speed of convergence toward MPP, instability around the GMPP and low efficiency. Therefore, in case of partial shading occurrence, where multiple peaks achieve almost similar output power. The algorithm can rapidly check the output power across those LMP, and determine which one the GMPP is. Thus obtaining highest possible efficiency in minimum computing time.

The fluctuation of temperature is a slow process, which takes span of hours. However, it can affect the performance of MPPT after locating the GMPP. To overcome the problem of reinitializing the EA-P&O unnecessarily, the algorithm measure the new current and compare it to the previously recorded. If the difference ($\frac{|I_{K-1}-I_K|}{I_{SC_{STC}}}$) is below 0.05, EA-P&O reevaluate the MPP using P&O based on Langrange interpolation mechanism within the same GMP region. Otherwise, it determine the occurrence of possible partial shading.

It is presented mathematically in [23], when G starts changing, the relation between two consecutive samples scanned by MPPT is:

$$\frac{\Delta P}{P} = \frac{\Delta G}{G_{STC}} \tag{2.25}$$

Thus, if $\Delta G/G_{STC} \geq 0.05$ (50 W/m^2), the threshold for normalized power can be calculated as $\Delta P/P=\Delta G/GSTC = (50/1000) = 0.05$. In Fig. 2.18, EA-P&O continuously checks for whether $\Delta P/P>0.05$ or not. If it is bigger than that, then EA-P&O entertain the possibility of occurring irradiance change with high rate, thus reinitializing the MPPT algorithm is required.

2.5 Conclusion

Several MPPT techniques have been introduced in this chapter. The main difference between classical and advanced methods is the later ability to converge to GMPP under non-uniform circumstances, which was inspired by numerous living organisms' behavior in nature.

At the end, an algorithm was proposed as an alternative solution for the primary limitations of the classical P&O technique. It retained its simple structure while mimicking the performance of metaheuristic methods, such as PSO and GWO, to locate GMPP in partial shading conditions. Incorporating a numerical technique to estimate the position of MPP also decreased its convergence time. In the next chapter, the proposed algorithm is evaluated against other methods.

CHAPTER 3 : Simulation and Results

3.1 Introduction

To assess the effectiveness of the proposed techniques, Matlab and Simulink are used to simulate a simple stand-alone system subjected to several atmospheric conditions. Then a comparative study with other algorithms in terms of robustness, tracking speed and efficiency is provided at the end of this chapter.

3.2 System Overview

The Simulink model of our system is illustrated in figure 2.4. It consist essentially of four serially connected PV modules of the same type Soltech 1STH-215-P, a boost converter driven by an MPPT controller, and a load of 20Ω.

3.3 DC-DC boost converter design:

Using the results of Section 1.8, and setting the switching frequency to 5 Hz , the components of the power converter are selected as it was shown in table 2.1.

It is worth mentioning that in order to get accurate measurements of the output PV power that corresponds to each duty cycle, the time interval between two successive transmissions of D should be greater than the boost converter settling time. To do so, several values of the duty cycle have to be tested to analyze the transient response of the power converter and the time it takes to settle down. After performing this evaluation, we have found that a sampling time of 0.008s is appropriate for our system.

3.4 Simulation Results

To verify the working principles of the EA-P&O, a set of tests is designed that comprises of a sudden irradiance change after uniform irradiance, partial shading that result in creating multiple peaks with almost similar output power, and an abrupt change in temperature. The assessment is implemented on a PV array consist of 4 modules (1Soltech 1STH-215-P) in a string. The irradiance G varies for a duration of 4 seconds. In the beginning, G=1000 W/m^2 and continued for 2 seconds. Afterwards it falls to 500 W/m^2 and persist for another 2 s. Then G change instantly as the partial

shading takes place for another 2 seconds. In Fig. 3.1 (a), the partial shading curve is presented. The PV array is shaded with 4 different levels of G (1000, 700 460 & 350W/m^2) that manifests the four peaks on the curve, where three LMP have close proximity GMP. Immediately after 6 seconds, a new partial shading occurs by irradiance levels of G (1000, 800 400 & 250 W/m^2), which is depicted in In Fig. 3.1 (b) where a distinct GMP can be distinguished from the remaining three LMP. At 7.98 seconds, the temperature rise from 25 ℃ up to 35 ℃ at t=8 seconds for the last 1 s.

In Fig. 3.2, V_{PV} depicts the tracking profile of EA-P&O. Some parts of the curves are enlarged to clarify the behaviour of the algorithm at the transients in Fig. 3.3. It can be seen in Image 1, that initially EA-P&O start scanning at $0.65V_{MPP} + 0.8V_{OC}*(N-1)$ recording current and then compare it with the current measured at 0.65 V_{OC}, thus the result yield no partial shading occurrence. The algorithm determine the location of the GMP at the last region using ($0.65 \times V_{OC\_}$ array) and start reducing the perturbation size as it reach the MPP until it settles at 37.99 V.

EA-P&O keeps on tracking the MPP for 2 s and then G falls to 500 W/m^2. This large variation in G induce large deviation in normalized power. Thus ($\Delta P/P$) is obviously greater than the 0.05. Thus, large power deviation checking condition is satisfied and partial shading occurrence checking is initiated. As the mechanism described above, the EA-P&O scans two points on the curve $0.65V_{MPP} + 0.8V_{OC}*(N-1)$ = 36.85 V, and $0.65V_{OC}$ =7.14 V. The voltage during this scan can be seen in image 2. The recorded current can be found as 3.81 A and 3.91 A at $0.65V_{MPP} + 0.8V_{OC}*(N-1)$ and $0.65V_{OC}$ respectively. During initialization, EA-P&O got the I_{SC} as 7.84 A and IMPP as 7.35 A for 1Soltech 1STH-215-P modules as an input from datasheet. After scanning the two points, EA-P&O deduce the valued of G1 and G2 by (2.19) and (2.20) respectively as ($3.81/7.35 \times 1000 = 518.4$ W/m^2) and ($3.91/7.84 \times 1000 = 498.7$ W/m^2). Difference between these two-calculated values of G is approximately 20 W/m^2. As the discrepancy is below than 50, EA-P&O will decide that the power change is due to the variation of G not partial shading. After acknowledging the fact that the irradiance level is changed, the EA-P&O goes straight back to track the MPP at ($48.4 \times 0.8 = 38.72$) V and start tracking the MPP at 39.05 V. In absence of such mechanism, usual MPPT scheme will consider it as a partial shading case and initiate a global peak searching unnecessarily.

After 2 s, the irradiance G across the four PV panels change, and partial shading takes place. The transient tracking of EA-P&O under partial shading is illustrated in image 3 from 4 s to 4.7 s. In can be seen from the VPV that, due to the large drop in power, EA-P&O initiate the partial shading checking by scanning the $0.65V_{MPP} + 0.8V_{OC}*(N-1)$ (36.7 V) and $0.65V_{OC}$ (7.03 V). The corresponding current at $0.65V_{MPP} + 0.8V_{OC}*(N-1)$ is 2.73 A, and $0.65V_{OC}$ is 7.79 A, can be found from I_{PV} in Fig. 3.4. Thus, the EA-P&O calculated the G1 and G2 at $0.65V_{MPP} + 0.8V_{OC}*(N-1)$ as $(2.73/7.35 \times 1000) = 371 W/m^2$ and at $0.65V_{OC}$ is $(7.79/7.84 \times 1000) = 993 W/m^2$. The difference between the values of G at these two points is 622 W/m^2 (more than 50).

As a consequence, EA-P&O decides that partial shading occurs and initiate searching under partial shading. The algorithm initiates scanning the current according to the 0.65Voc model. Following that model EA-P&O is supposed to scan the 2 remaining points 15.59 and 25.64 V. To comprehend the procedure, the current notations on IPV curve should be considered. A sharp fall of current at sample 1 and 2 occur that help realize right shifting of the V_{MPP}. The algorithm revaluate the expected V_{MPP} at 2nd, 3rd and 4th regions and calculate the approximate LMP at the four peaks ending up with (2.21) (LMP1= 8.91V×7.79A= 69.48W, LMP2= 20.04V×5.47A= 111.8W, LMP3=31.38V×3.6A= 113W and LMP4= 42.24V×2.74A= 115.74W). EA-P&O compare the calculated power, and realize that 2nd, 3rd and 4th LMP satisfy the 10% criteria. As a result, it checks the real LMP values at those region starting with low perturbation size until it reach their MPP. Then, it compare the measured LMPs, and determine which region is the GMP before going back to it. This procedure discarded the first region from the searching list, while maintaining high power efficiency as shown in Image 3 from Fig.3.3 and Fig.3.5.

In the 6th second, different partial shading levels occur, which can be detected by EA-P&O through the deviation in power. Repeating the same steps mentioned above, whereas the algorithm measure the current and calculate the difference in G at $0.65V_{OC}$ and $0.65V_{MPP} + 0.8V_{OC}*(N-1)$ as:

$$G_1 - G_2 = \left(\frac{7.79}{7.84} - \frac{1.96}{7.35}\right) \times 1000 = 727\ \mathrm{W}/m^2 > 50\ \mathrm{W}/m^2$$

After, determining the partial shading occurrence the EA-P&O scan the current at 10.53V and 22.83V from (2.21) as shown in Image 4. The estimated LMP after taking the right shift of the peaks into account yielded (LMP1= 8.91V×7.8A= 69.49W, LMP2= 20.55V×6.25A= 128.42W,

LMP3= 31.39V×3.13A= 98.25W and LMP4= 42.29V×1.96A= 82.88W), thus the GMP is distinguished directly at V_{GMP}=20.33V without initiating a global peak searching unnecessarily.

Finally at 7.98 s, the redundancy of EA-P&O under varying temperature conditions is tested, by changing the temperature uniformly across the panels by 10 ℃. The algorithm detect a power deviation with small current and voltage variation, as a result it only initialize the MPP searching mechanism within the same GMP region, as such the power output increase from 111W to 115.5W (image 5 from Fig. 3.3). The inclusion of this method provide a mean to differentiate between power deviation due to G variation and power deviation because of sudden temperature fluctuation as depicted in Fig.3.6.

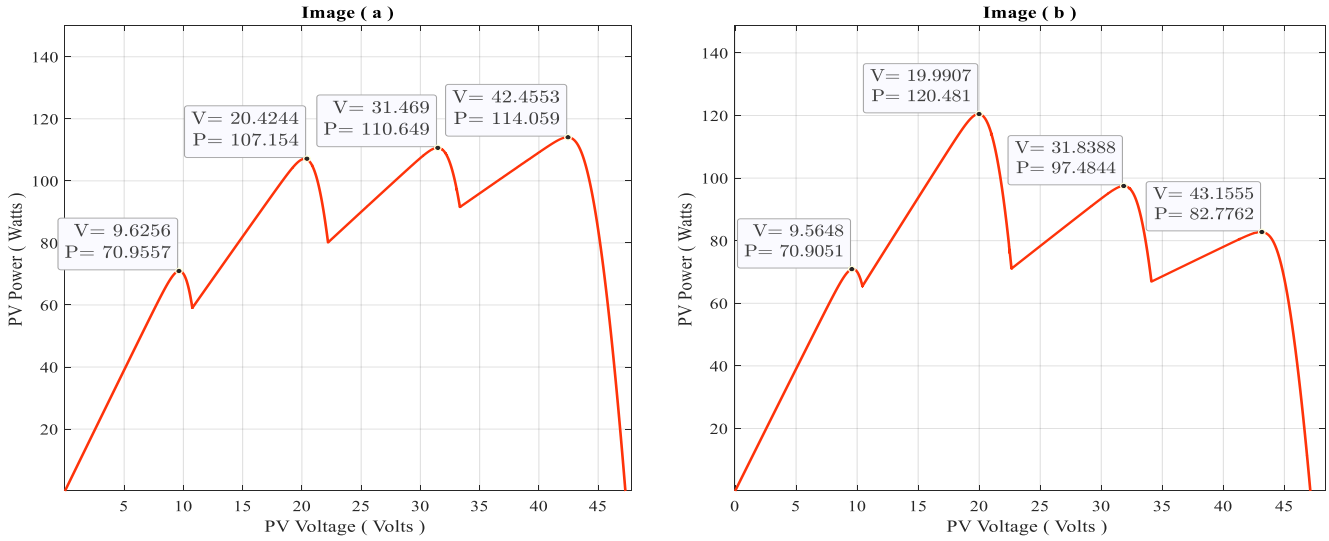

Figure 3.1: P-V Curves under partial shading

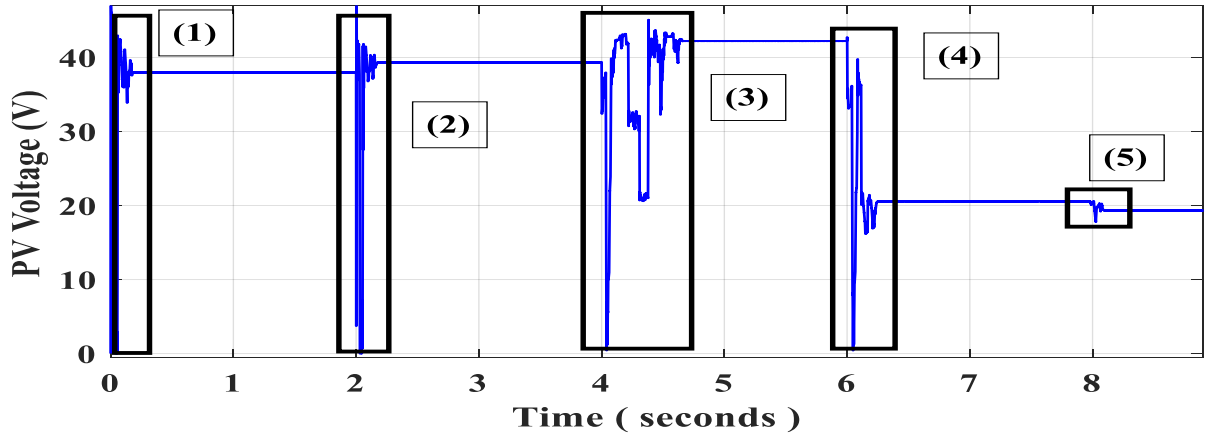

Figure 3.2: PV Voltage Curve of EA-P&O

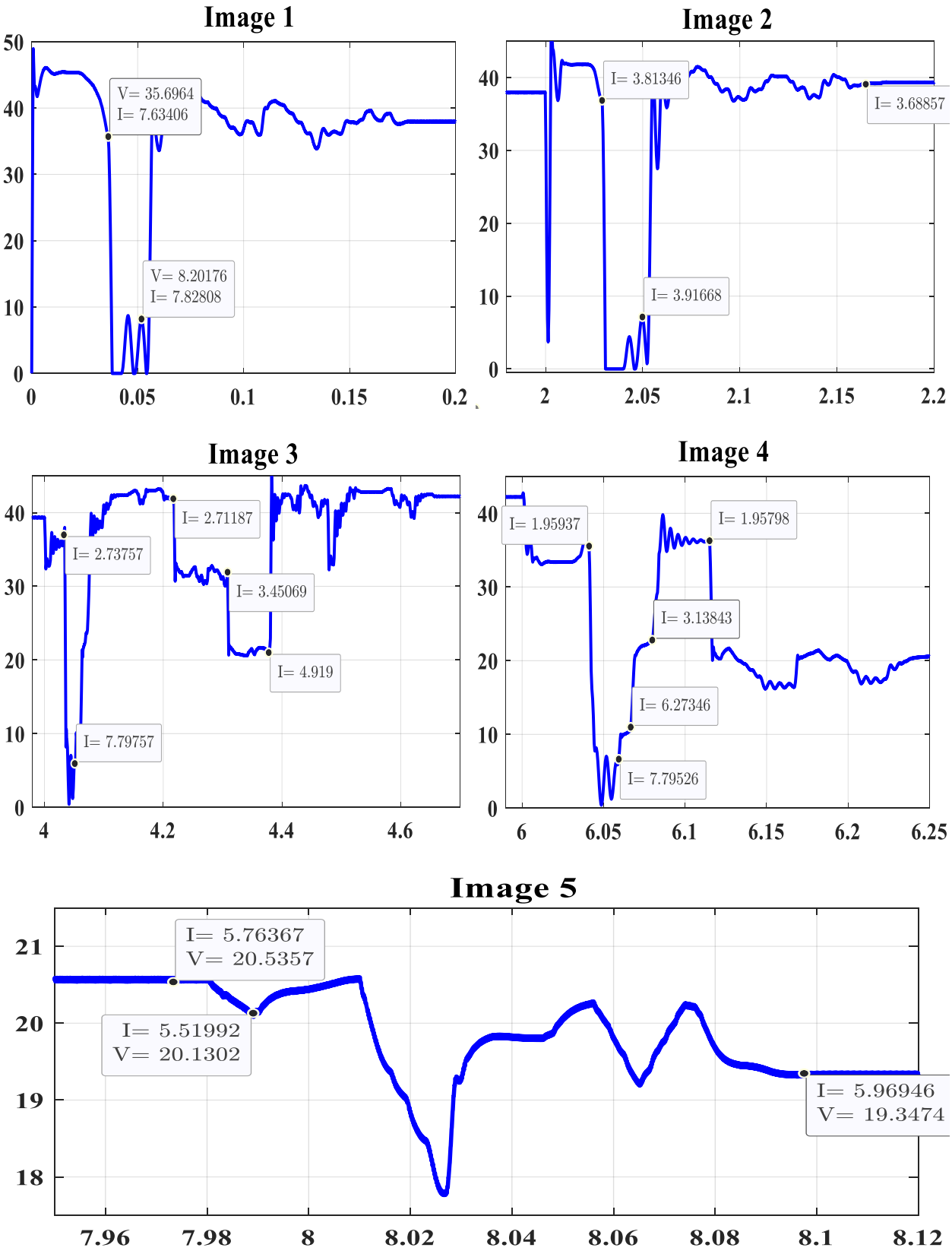

Figure 3.3: Enlarged PV Voltage Curve of EA-P&O at the transients

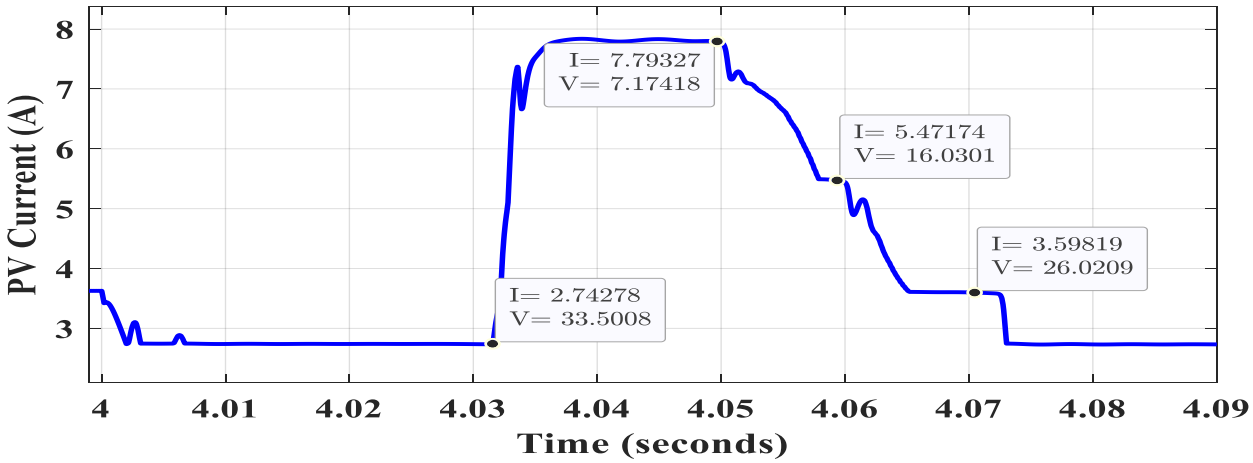

Figure 3.4: PV Current Curves of EA-P&O

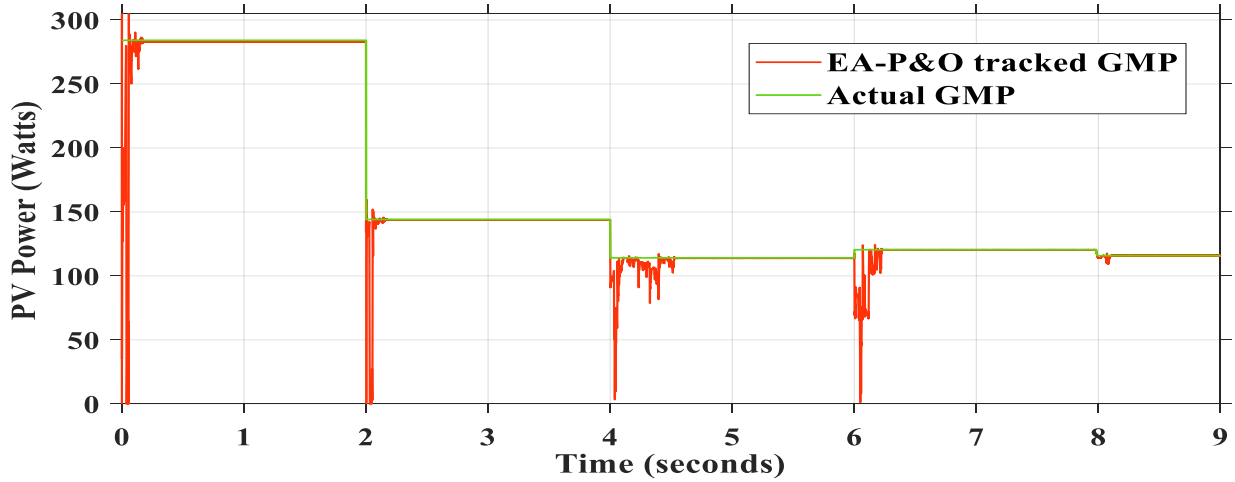

Figure 3.5: PV Power Curve of the EA-P&O

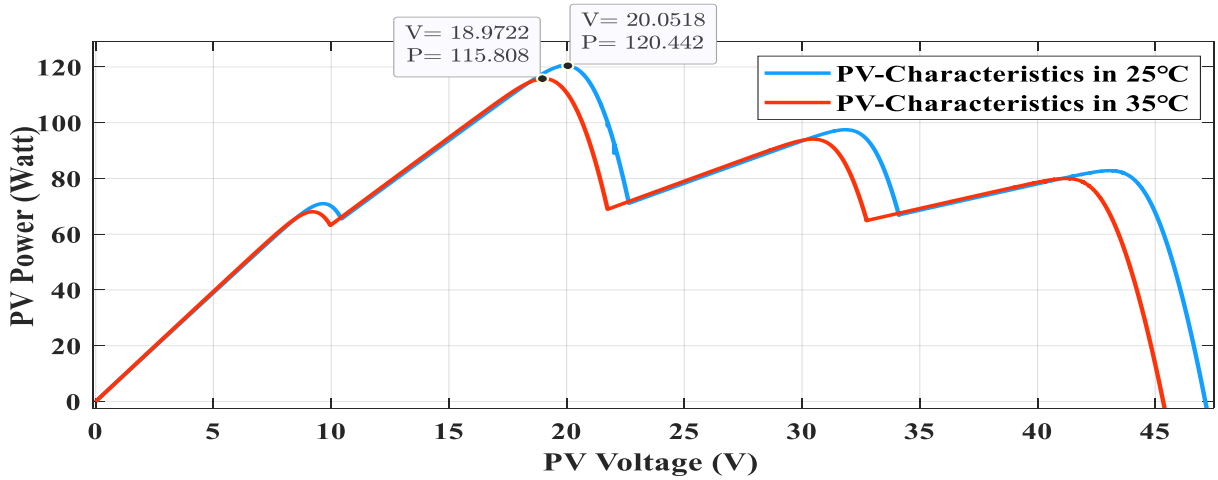

Figure 3.6: P-V characteristic Curves in 25℃ and 35℃

3.5 Comparisons with Other MPPT

The performance of the proposed EA-P&O is evaluated against two previously mentioned MPPT techniques, namely Particle Swarm Optimization (PSO) and Grey Wolf Optimization (GWO).

Table 3.1 provides the selected parameters of every optimizer, the reader should notice that the settings may differ to that provided in the original papers of these algorithms which might be unsuitable for MPPT applications. The selection of the population size N has a significant impact on the performance of the optimizer. A large N will improve the search ability and tracking accuracy; however, it will increase the convergence time of the algorithm. On the other hand, a small N speeds up the search process, but it may lead to poor power efficiency.

In this work, and in order to make a fair comparison, we have selected N to be 4, which seems to be a reasonable choice. The maximum number of iterations is set to 11 for both PSO and GWO algorithms.

Table 3.1: Algorithmes Parametrization

Algorithms	***Parametrization***
PSO	$\omega = 0.4 c_1 = 1.4 \quad c_2 = 2$
GWO	$a = 0.7 - 0.7t/T$

In this section of the chapter, the switching frequency is raised to 50 kHz, but the same sampling time is maintained with other system specifications, as indicated in Table 3.2. By raising the number of Soltech 1STH-215-P PV modules to six connected in series, the complexity of the resulting PV characteristic curve patterns can be manipulated. As a result, six possible MPPs in the final curves can be observed. The simulation design parameters are modified in order to get accurate measurements of the output PV power that corresponds to each duty cycle.

Table 3.2: DC-DC Converter Components Selection for System 2

Switching Frequency	Inductor (L)	Input Capacitor	Output Capacitor
50 kHz	10 mH	100μF	100μF

3.5.1 Results and Discussion

Six distinct scenarios have been subjected to the PV system. In the first case, the PV array receives a fast varying uniform irradiance that changes every 0.5 seconds in three different levels: 500-1000-750 *W/m²*. In the five remaining cases, different partial shading patterns with various numbers of peaks have been exposed to the substrings that constitute the six PV modules. Table 3.3 and figure illustrate the different scenarios and their PV characteristics.

Table 3.3: Studied Irradiance conditions

Cases	***Irradiance levels distribution on the modules Substrings (W/m²)***	***GMPP (W)***
1: Uniform Fast Varying Irradiance	[0s,0.5s]:500 [0.5s,1s]:1000 [1s,1.5s]:750	216.2 426.3 322.9
2: PSC	800/800/600/600/300/300	183.196
3: PSC	1000/1000/800/600/300/300	192.774
4: PSC	1000/800/800/600/400/300	191.184
5: PSC	1000/800/700/600/500/300	201.93
6: PSC	1000/900/800/700/600/500	245.1681

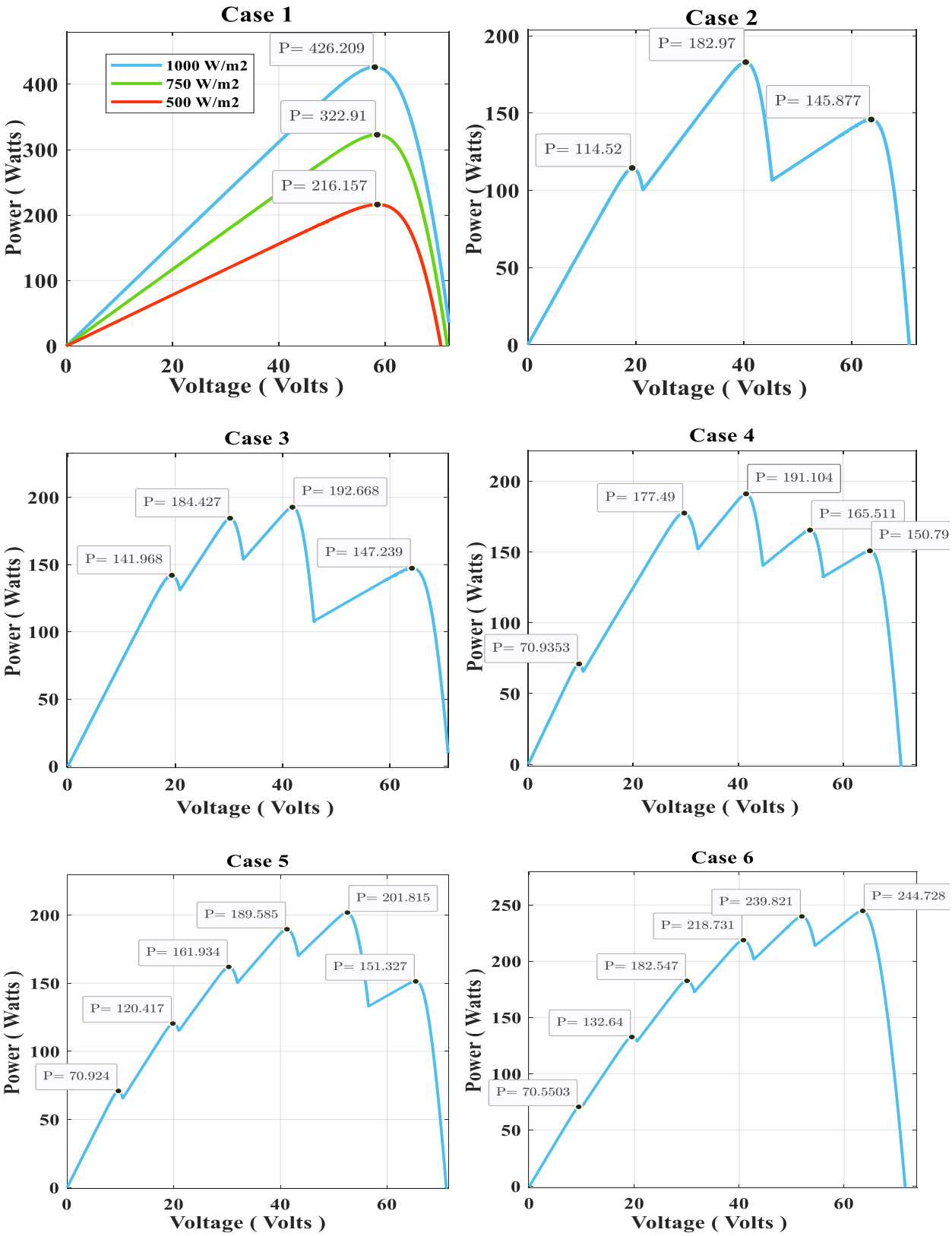

Figure 3.7: P-V Characteristic Curves of the Studied Cases

3.5.1.1 Uniform Fast Varying irradiance

The resulting PV power curves for each algorithm with uniform fast varying irradiation are shown in figure 3.8. All algorithms were able to detect changes in irradiation levels, and locate the maximum power point. Table 3.4 provides the results details of the simulation in terms of efficiency and time convergence in each time interval

Table 3.4: Steady State Tracking Results under Fast Varying Uniform Irradiance

Optimizer	GMPP(W)	Tracked Power (W)	Convergence Time (s)
EA-P&O	216.2 426.3 322.9	216 - 425.59 - 322.9	0.184-0.184-0.232
PSO		212.53 - 419.82 - 322.9	0.352-0.352-0.32
GWO		183.14 - 426.14 - 322.9	0.352-0.32-0.352

In order to have a better assessment measure, we consider the average efficiencies and average convergence time as provided in table 3.5.

Table 3.5: Average Efficiencies and Convergence Time under Fast Varying Uniform Irradiation

Optimizer	Average Efficiency	Average Convergence Time
EA-P&O	99.91	0.2
PSO	98.93	0.341
GWO	94.89	0.341

It can be observed, that all algorithms have high efficiencies. Where EA-P&O being fastest with highest efficiency, while GWO and PSO have nearly equal speed with considerable difference in efficiency.

3.5.1.2 Non-uniform Irradiance levels

Figures 3.9, 3.10, 3.11, 3.12, 3.13 depict the obtained power curves under partial shading conditions in cases 2 through 6, and table 3.6 provides the resulting steady state static efficiencies and tracking times.

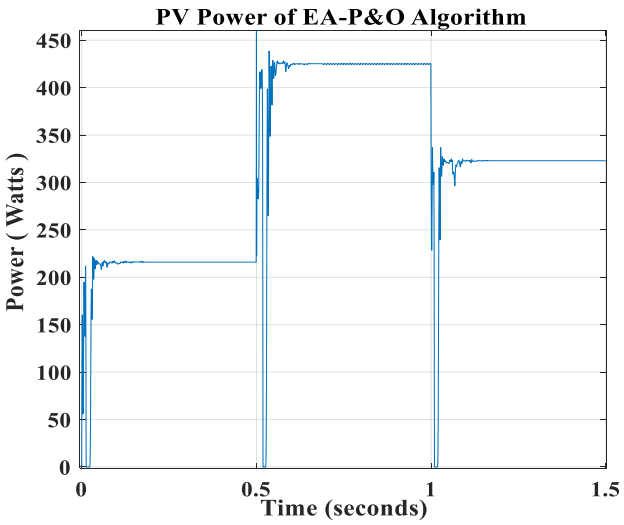

Figure 3.8: PV Power Curves of Case 1

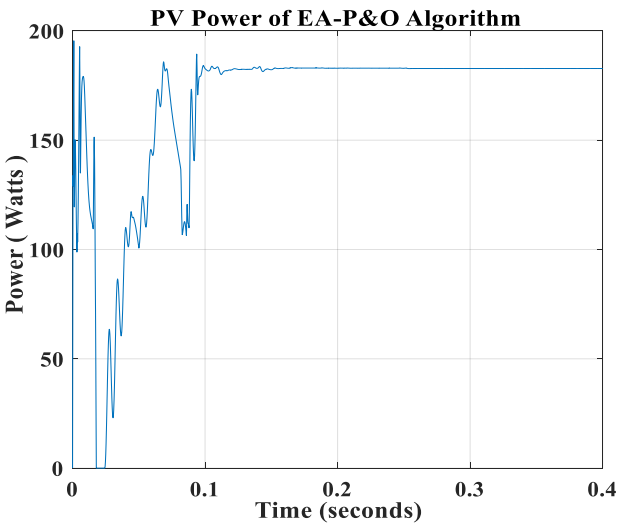

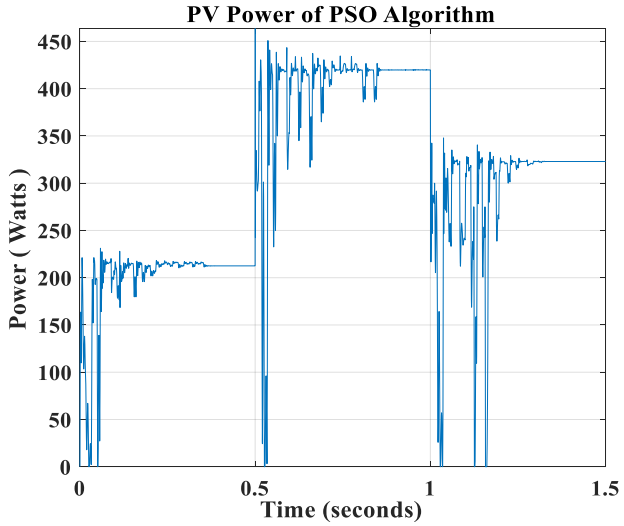

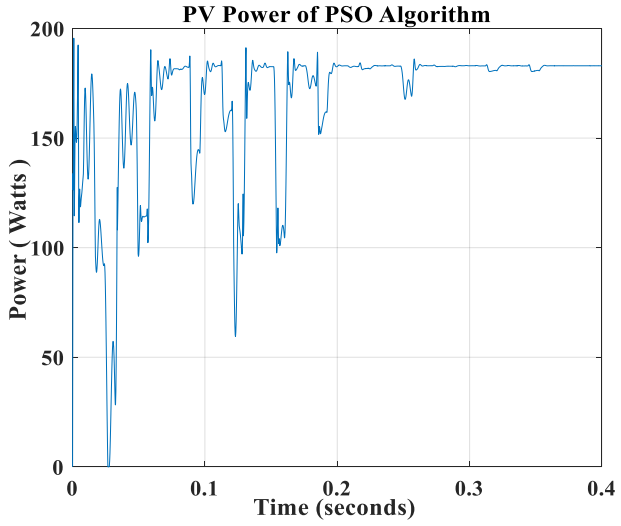

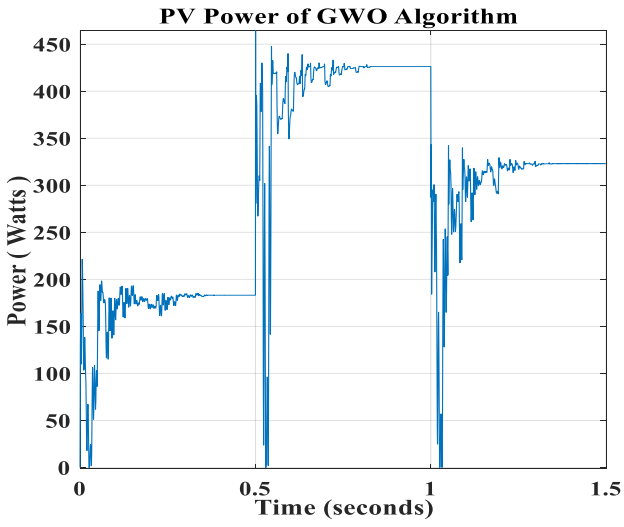

Figure 3.9: PV Power Curves of Case 2

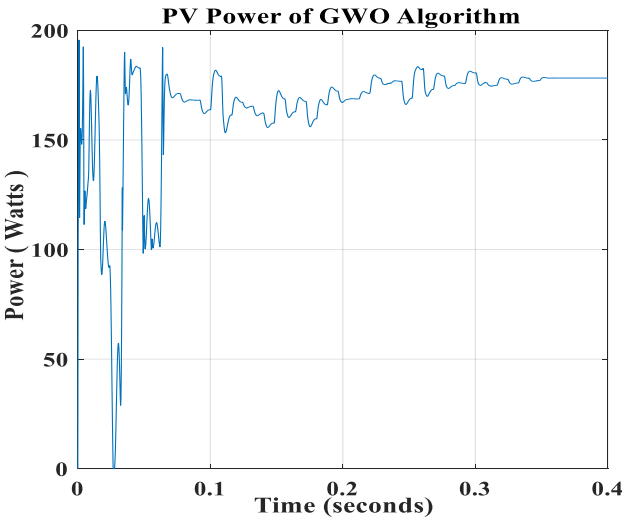

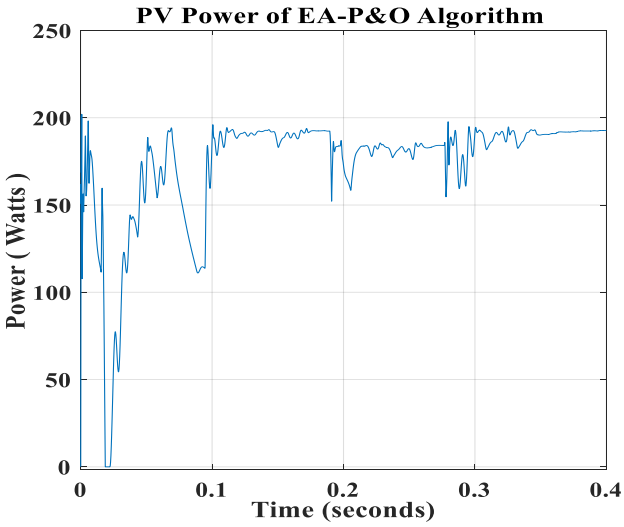

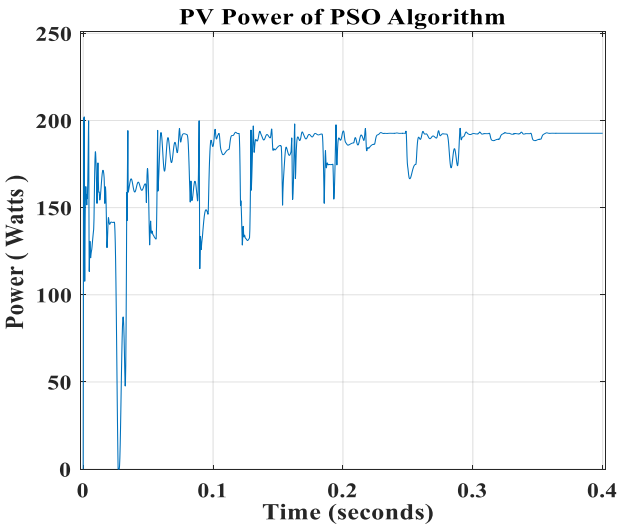

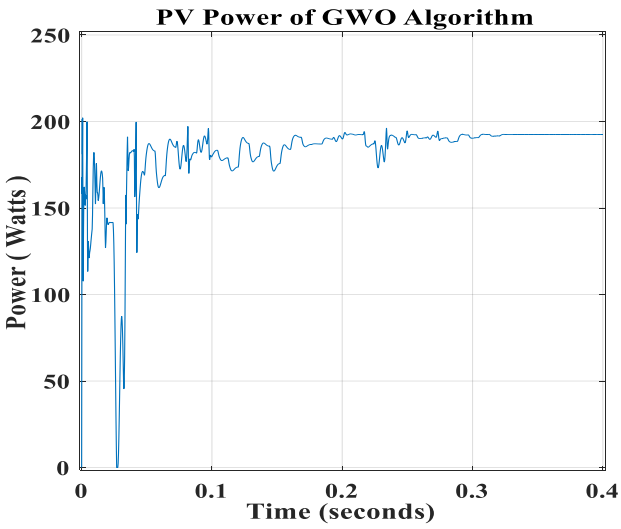

Figure 3.10: PV Power Curves of Case 3

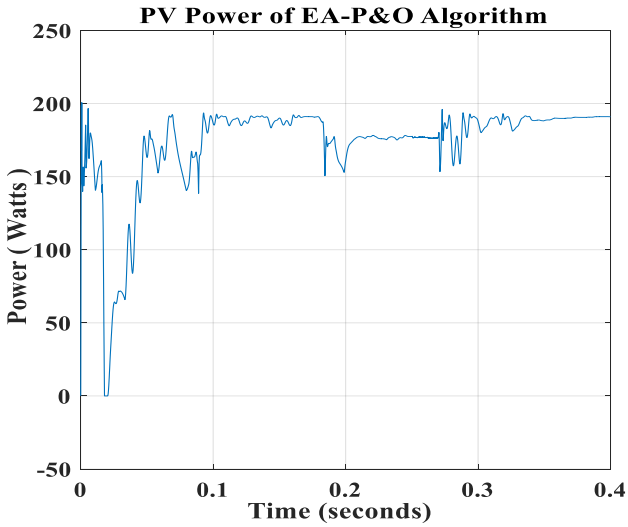

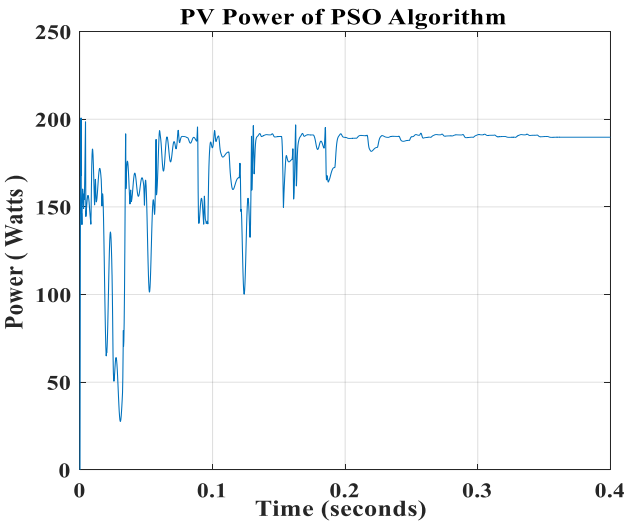

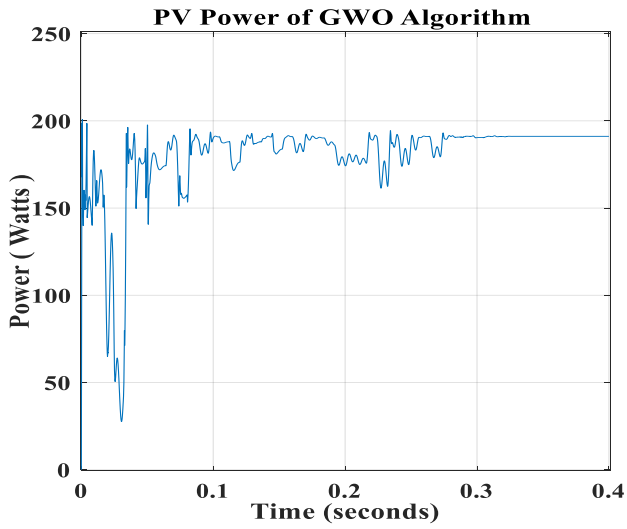

Figure 3.11: PV Power Curves of Case 4

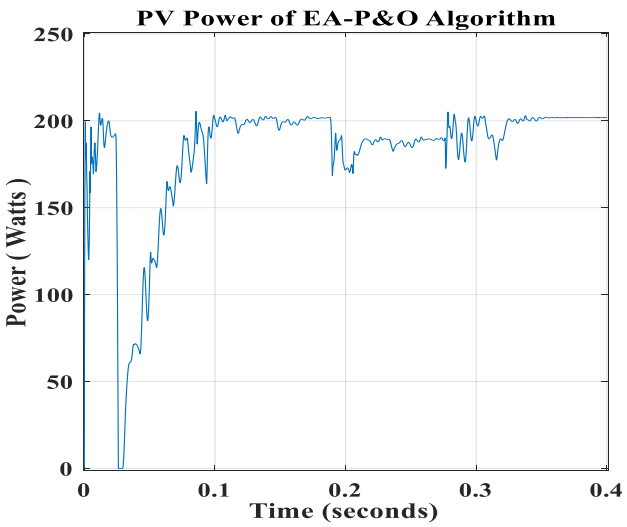

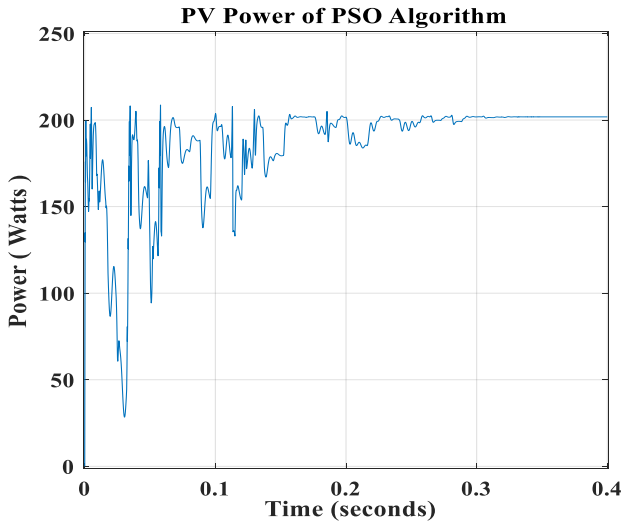

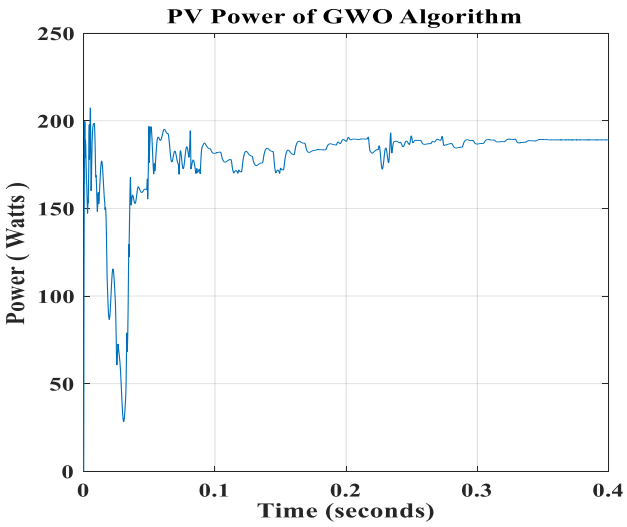

Figure 3.12: PV Power Curves of Case 5

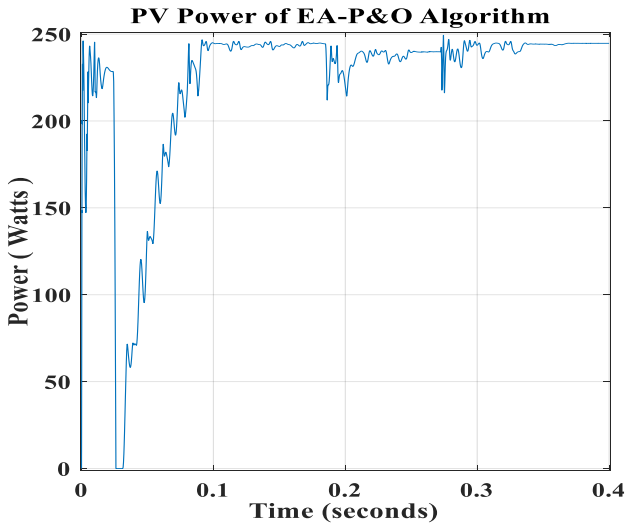

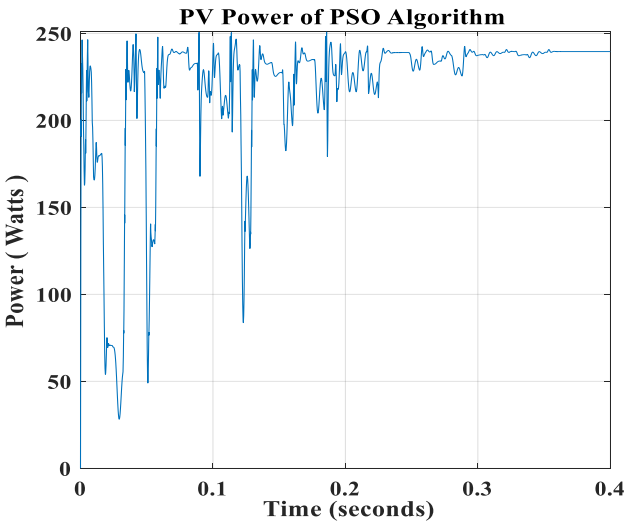

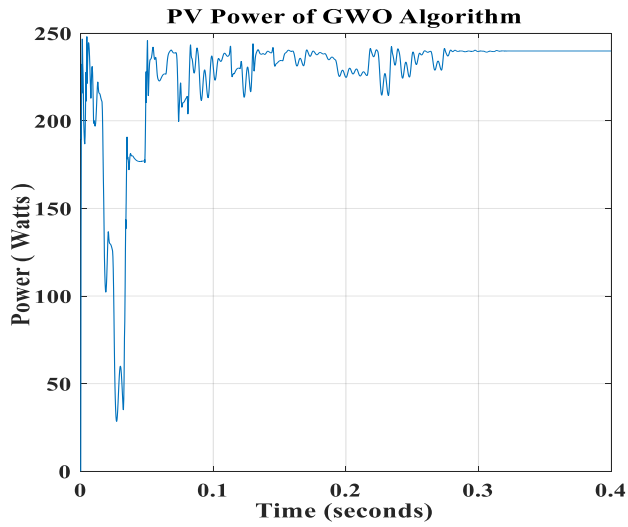

Figure 3.13: PV Power Curves of Case 6

Table 3.6: Steady State Tracking Results under Non Uniform Irradiance

Cases	Optimizer	GMPP(W)	Tracked Power (W)	GMPP Located	Accuracy (%)	Convergence Time (s)
2	EA-P&O	183.196	182.93	Yes	99.85	0.168
	PSO		182.99	Yes	99.89	0.352
	GWO		178.25	Yes	97.3	0.352
3	EA-P&O	192.774	192.64	Yes	99.93	0.328
	PSO		192.68	Yes	99.95	0.352
	GWO		192.45	Yes	99.83	0.32
4	EA-P&O	191.184	191.03	Yes	99.91	0.368
	PSO		189.74	Yes	99.24	0.352
	GWO		191.18	Yes	99.99	0.32
5	EA-P&O	201.93	201.81	Yes	99.94	0.352
	PSO		201.83	Yes	99.95	0.32
	GWO		189.1	**No**	93.65	0.352
6	EA-P&O	245.1681	244.67	Yes	99.79	0.368
	PSO		239.54	**No**	97.7	0.352
	GWO		239.81	**No**	97.81	0.32

- It can be observed that the EA-P&O, PSO and the GWO scored almost high accuracies, and successfully located the GMPP associated with the 2nd, 3rd and 4th case. In the second case, the GWO obtained the worst accuracy (97.3%), compared to the best one (99.89%). Also The EA-P&O achieved the lowest Convergence Time of 0.168 second among the cases of non-uniform irradiance.
- The GWO got the lowest power level in the third case at which it achieved 192.45W out of 183.196W resulting in an accuracy of 99.83% compared to the highest rank (99.95%).
- The best result obtained by the GWO algorithm was in 4th case at which it obtained an accuracy 99.99% which can be ranked at the 1st position in descending order across all cases.
- The GWO algorithm in the other hand have stagnated at the fourth and fifth local maximum associated with the 5th and 6th shading patterns (189.1 W out of 201.93 W in case 5 and

239.81 W out of 245.1681 W in case 6). The PSO have also stagnated at the fifth local maximum in case 6 (239.54 W out of 245.1681 W).

- In terms of convergence speed, it can be clearly seen that the EA-P&O is the fastest among the remaining algorithms in case 2 where a distinct GMPP have a difference of more than 10% with the next highest LMP. Using this strategy, the algorithm has high prospects of exploring promising regions rapidly, hence undesirable areas are discarded along the optimization process, this result in an efficacious transition from diversification into intensification, which grant the algorithm the ability to locate GMPP as in case 6 despite the difficulty GWO and PSO face to distinguish it among other LMPs.

Table 3.7 provides the average acurracies and average settling times obtained by the assessed techniques:

Table 3.7: Average Accuracies and Convergence Time under Non Uniform Irradiation

Optimizer	Average Accuracies (%)	Average Convergence Time(s)
EA-P&O	99.88	0.316
PSO	99.35	0.345
GWO	97.7	0.332

3.6 Conclusion

This chapter was devoted to the evaluation of EA-P&O algorithms in Maximum Power Point Tracking. Simulink and Matlab were used to design and simulate a standalone PV system driven by an MPPT controller and subjected to various atmospheric conditions. The algorithm was assessed in varying scenarios of fast varying uniform and non-uniform irradiance and ambient temperature. Then, it was subjected with other metaheuristic to 6 distinct cases of fast varying uniform and non-uniform irradiation, accompanied with the resulting power curves and necessary tables. The analyses of the simulation results of the studied cases, have demonstrated the effectiveness of the proposed algorithms in handling various challenging shading patterns, and achieved the high accuracy levels in all cases over the remaining popular stochastic algorithms. Moreover, the proposed method are characterized by fast tracking speed under varying uniform irradiance, this was conspicuous in the convergence time of the EA-P&O which was 0.2s on average outperforming the remaining algorithms, while being a powerful competitor with nearly identical settling times of 0.31 seconds in most of the non-uniform cases.

General Conclusion and Future Work:

The quest for sustainable and efficient energy solutions has driven significant advancements in photovoltaic (PV) technology. This project aimed to enhance the performance of PV systems, especially under Partial Shading Conditions (PSCs), by implementing advanced Maximum Power Point Tracking (MPPT) algorithms. Our research evaluated the effectiveness of traditional MPPT techniques such as Perturb and Observe (P&O) and Incremental Conductance (IC), alongside modern algorithms like Particle Swarm Optimization (PSO) and Grey Wolf Optimizer (GWO). Additionally, we introduced an Enhanced Adaptive P&O (EA-P&O) algorithm to improve tracking accuracy and efficiency under PSCs.

The results indicated that while classical methods are straightforward and easy to implement, they often fail to locate the global maximum power (GMP) under PSCs, leading to unsatisfactory performance. In contrast, advanced algorithms like PSO and GWO demonstrated superior ability to identify the GMP, thereby enhancing the overall power output of the PV system. The EA-P&O algorithm, in particular, showed significant improvement in tracking speed and accuracy, effectively overcoming the limitations of conventional techniques.

Our findings highlight the critical importance of adopting advanced MPPT algorithms in real-world PV systems to maximize energy harvest, especially in environments prone to partial shading. The implementation of these algorithms can result in more reliable and efficient solar energy systems, contributing to the broader goal of sustainable energy development.

Despite the promising results, the study also identified certain limitations. The simulation tests, although comprehensive, cannot fully replicate all possible real-world conditions. Future research should focus on field-testing these algorithms to validate their performance across diverse environmental scenarios. Additionally, further investigation into hybrid algorithms combining the strengths of multiple techniques could yield even more robust solutions for MPPT under varying conditions.

References:

[1] International Renewable Energy Agency (IRENA), "Renewable Power Generation Costs in 2020," IRENA, Abu Dhabi, 2021. Available:https://www.irena.org//media/Files/IRENA/Agency/Publication/2021/Jun/IRENA_Power_Generation_Costs_2020_Summary.pdf. [Accessed: June 11, 2024].

[2] "Different Types of Solar PV Systems," Deege Solar. [Online]. Available: https://www.deegesolar.co.uk/different_types_of_solar_pv_systems/. [Accessed: 04-June-2024].

[3] C. S. Solanki, "*Solar Photovoltaic Technology and Systems: A Manual for Technicians, Trainers and Engineers*," PHI Learning, 2013.

[4] M. Tanrioven, "*Photovoltaic Systems Engineering for Students and Professionals: Solved Examples and Applications,"* CRC Press, 2023.

[5] M. Dhimish, "Assessing MPPT techniques on hot spotted and partially shaded photovoltaic modules: Comprehensive review based on experimental data," IEEE Access, vol. 8, pp. 110-122, Jan. 2020.

[6] Muhammad H. Rashid, "*Power Electronics Devices, Circuits, and Applications,"* 4th ed., Pearson, 2014.

[7] A. Belkaid, I. Colak, and K. Kayisli, “Implementation of a modified P&O-MPPT algorithm adapted for varying solar radiation conditions,” Electr. Eng., vol. 99, no. 3, pp. 839–846, 2017.

[8] . Sumathi,L. Ashok Kumar,P. Surekha, Solar PV and Wind Energy Conversion Systems: An Introduction to Theory, Modeling with MATLAB/SIMULINK, and the Role of Soft Computing Techniques, 2017, journal, pages.

[9] Ke-Lin Du, M. N. S. Swamy, Search and Optimization by Metaheuristics: Techniques and Algorithms Inspired by Nature, 2016, vol. year, journal, pages.

[10] D.P. Holm, M.E. Ropp, “Comparative study of maximum power point algorithm,” Progress in Photovoltaics: Research and Applications, vol. 11, no.1, pp. 47-62, Jan. 2003.

[11] Z.Yan, L. Fei, Y.Jinjun and D.Shanxu, “Study on realizing MPPT by improved incremental conductance method with variable step size,” Proc. IEEE ICIEA, pp. 547-550, 2008.

[12] Performance of PV Topologies under Shaded Conditions, SolarEdge.

[13] J. Kennedy, R.C. Eberhart, et al. Particle swarm optimization. In Proceedings of IEEE international conference on neural networks, volume 4, pages 1942–1948. Perth, Australia, 1995.

[14] An improved PSO-based MPPT control strategy for photovoltaic systems - Scientific Figure on ResearchGate. Available from: https://www.researchgate.net/figure/Movement-of-particles-in-the-optimization-process_fig9_275594385 [accessed 12 Jun, 2024]

[15] Faris, H., Aljarah, I., Al-Betar, M.A. et al. Grey wolf optimizer: a review of recent variants and applications. Neural Comput & Applic 30, 413–435 (2018). https://doi.org/10.1007/s00521-017-3272-5

[16] Grey wolf optimizer: a review of recent variants and applications - Scientific Figure on ResearchGate. Available from: https://www.researchgate.net/figure/Social-hierarchy-of-grey-wolves_fig4_321294919 [accessed 11 Jun, 2024]

[17] Grey Wolf Optimizer - Scientific Figure on ResearchGate. Available from: https://www.researchgate.net/figure/Hunting-behaviour-of-grey-wolves-A-chasing-approaching-and-tracking-prey-B-D_fig1_260010809 [accessed 11 Jun, 2024]

[18] Mirjalili, S. M. and Andrew P. Lewis. “Grey Wolf Optimizer.” Adv. Eng. Softw. 69 (2014): 46-61.

[19] Zhang, Sen & Luo, Qifang & Zhou, Yong-Quan. (2017). Hybrid Grey Wolf Optimizer Using Elite Opposition-Based Learning Strategy and Simplex Method. International Journal of Computational Intelligence and Applications. 1750012. 10.1142/S1469026817500122.

[20] K. Sundareswaran, V. Vigneshkumar, P. Sankar, S. P. Simon, P. S. R. Nayak, and S. Palani, “Development of an improved P&O algorithm assisted through a colony of foraging ants for MPPT in PV system,” IEEETrans. Ind. Informat. vol. 12, no. 1, pp. 187–200, Feb. 2016.

[21] C. Manickam, G. P. Raman, G. R. Raman, S. I. Ganesan, and N. Chilakapati, “Fireworks enriched P&O algorithm for GMPPT and detection of partial shading in PV systems,” IEEE Trans. Power Electron., vol. 32, no. 6, pp. 4432–4443, Jun. 2017.

[22] S. Mohanty, B. Subudhi, and P. K. Ray, “A grey wolf-assisted perturb & observe MPPT algorithm for a PV system,” IEEE Trans. Energy Convers., vol. 32, no. 1, pp. 340–347, Mar. 2017.

[23] J. Ahmed and Z. Salam, “A modified P&O maximum power point tracking method with reduced steady-state oscillation and improved tracking efficiency,” IEEE Trans. Sustain. Energy, vol. 7, no. 4, pp. 1506–1515, Oct. 2016.

[24] C. Rahmann, V. Vittal, J. Ascui, and J. Haas, “Mitigation control against partial shading effects in large-scale PV power plants,” IEEE Trans. Sustain. Energy, vol. 7, no. 1, pp. 173–180, Jan. 2016

[25] H. Patel and V. Agarwal, “Maximum power point tracking scheme for PV systems operating under partially shaded conditions,” IEEE Trans. Ind. Electron., vol. 55, no. 4, pp. 1689–1698, Apr. 2008.

[26] A. Kouchaki, H. Iman-Eini, and B. Asaei, “A new maximum power point tracking strategy for PV arrays under uniform and non-uniform insolation conditions,” Sol. Energy, vol. 91, pp. 221–232, May 2013.

[27] J. Ahmed and Z. Salam, “An accurate method for MPPT to detect the partial shading occurrence in a PV system,” IEEE Trans. Ind. Informat. vol. 13, no. 5, pp. 2151–2161, Oct. 2017.

[28] Y.-H. Liu, J.-H. Chen, and J.-W. Huang, “A review of maximum power point tracking techniques for use in partially shaded conditions,” Renewable Sustain. Energy Rev., vol. 41, pp. 436–453, Jan. 2015

[29] J. Ahmed and Z. Salam, “An improved method to predict the position of maximum power point during partial shading for PV arrays,” IEEE Trans. Ind. Informat., vol. 11, no. 6, pp. 1378–1387, Dec. 2015.

[30] G. L. Jin, A. Ibrahim, Y. K. Chean et al., “Evaluation of single-pass photovoltaic-thermal air collector with rectangle tunnelabsorber,”American Journal of Applied Sciences, vol. 7, no. 2,pp. 277–282, 2010.

[31] M. Noro, R. Lazzarin, and G. Bagarella, “Advancements in hybrid photovoltaic-thermal systems: performance evaluations and applications,”Energy Procedia, vol. 101, pp. 496–503, 2016

[32] . Piegari and R. Rizzo, “Adaptive perturb and observe algorithm for photovoltaic maximum power point tracking,” IET Renew. Power Gener., vol. 4, no. 4, p. 317, 2010.

[33] Ramdan B. A. Koad, Ahmed Faheem Zobaa, “A Novel MPPT Algorithm Based on Particle Swarm Optimization for Photovoltaic Systems”,IEEE Transaction on sustainable energy, vol. 8, no. 2, April 2017